Received: 11 September 2023 | Revised: 10 January 2024 | Accepted: 10 January 2024

DOI: 10.1002/appl.202300085

MINI REVIEW

Applied Research

Inkjet-printed flexible *MXetronics*: Present status and future prospects

Rajavel Krishnamoorthy[1] | **Suprem R. Das**[1,2]

[1]Department of Industrial and Manufacturing Systems Engineering, Kansas State University, Manhattan, Kansas, USA

[2]Department of Electrical and Computer Engineering, Kansas State University, Manhattan, Kansas, USA

Correspondence
Suprem R. Das, Department of Industrial and Manufacturing Systems Engineering, Kansas State University, Manhattan, KS 66506, USA.
Email: srdas@ksu.edu

Funding information
National Science Foundation

Abstract

Over the past several years, atomically thin two-dimensional carbides, nitrides, and carbonitrides, otherwise known as *MXenes*, have been expanded into over fifty material candidates that are experimentally produced, and over one hundred fifty more candidates that have been theoretically predicted. They have demonstrated transformative properties such as metallic-type electrical conductivities, optical properties such as plasmonics and optical nonlinearity, and key surface properties such as hydrophilicity, and unique surface chemistry. In terms of their applications, they are poised to transform technological areas such as energy storage, electromagnetic shielding, electronics, photonics, optoelectronics, sensing, and bioelectronics. One of the most promising aspects of *MXene's* future application in all the above areas of interest, we believe, is reliably developing their flexible and bendable electronics and optoelectronics by printing methods (henceforth, termed as *printed flexible MXetronics*). Designing and manipulating *MXene* conductive inks according to the application requirements will therefore be a transformative goal for future printed flexible MXetronics. *MXene's* combined property of high electrical conductivity and water-friendly nature to easily disperse its micro/nano-flakes in an aqueous medium without any binder paves the way for designing additive-free highly conductive *MXene ink*. However, the chemical and/or structural and hence functional stability of water based *MXene* inks over time is not reliable, opening research avenues for further development of stable and conductive *MXene* inks. Such priorities will enable applications requiring high-resolution and highly reliable printed *MXene* electronics using state-of-the art printing methods. Engineering *MXene* structural and surface functional properties while tuning *MXene* ink rheology in benign solvents of choice will be a key for ink developments. This review article summarizes the present status and prospects of *MXene* inks and their use in inkjet-printed (IJP) technology for future flexible and bendable *MXetronics*.

KEYWORDS
additive manufacturing, conductive inks, inkjet printing, *MXene*, *MXetronics*

INTRODUCTION

Atomically thin two-dimensional (2D) materials have demonstrated a wide variety of electronic, optical, mechanical, thermal, chemical, and electrochemical properties since the discovery of graphene, with their electronic phase ranging from semi-metals to metals, semiconductors, insulators, magnetic, and superconducting in nature. *MXene* constitutes the largest subgroup within the 2D materials category—a subgroup that has exceptional promise in demonstrating 2D metallic conductivity (electronic), exceptional linear and nonlinear optical properties, high-optical transparency, fascinating plasmonic properties, hydrophilicity, unique electromagnetic interference properties, surface chemical properties that are key to applications such as electronics, photonics, optoelectronic switches, sensing, energy, separation and purification, and catalysis [1–7]. *MXene* carries a general chemical formula of $M_{n+1}X_nT_x$, with "M" as a transition metal atom (n = 1, 2, 3, and 4); "X" stands for carbon or nitrogen atom, and "T" represents a surface functional group such as -O, -F and/or -OH. Although to date over fifty 2D *MXene* candidates have been experimentally reported and over one hundred and fifty more are theoretically predicted, *MXene*'s controlled synthesis, stability, reliability, and applications remain a long-standing issue. Currently, materials discovery of *MXene* remains very attractive primarily due to the availability of large variety of transition metals, and their fascinating chemistries and electronic properties with carbon, nitrogen, and carbonitrides. Study of surface chemistries of MXene with associated functional moieties also constitutes another attractive areas of research in 2D MXene. One of the special properties of *MXene* is its hydrophilicity, which is both a blessing and as a curse. While the adhesion of water molecules makes *MXene* the most popular 2D material for large-scale aqueous-based material synthesis, water molecule also notoriously reacts with *MXene* oxidizing it to different phases of titanium oxide and other species, making this issue a topic of current research [8]. Generally, large-scale exfoliation of MXene via a top-down approach involves a selective metal etchant to etch suitable MAX phase materials followed by a liquid phase exfoliation using intercalation or a gentle agitation mechanism to delaminate the structure.

Nevertheless, the unique feature of *MXene* conductive inks relates to the hydrophilic nature of *MXene* nanosheets leading to stable colloidal suspension and to the retention of *MXene*'s exceptional electrical conductivity. While these properties expand the opportunity of making *MXene* materials as high quality conductive *MXene* inks, there exists number of opportunities both in fundamental material design and the corresponding ink synthesis. Beyond water, organic solvents possess great interest in extending the formulation of nonaqueous based *MXene* inks. As such, *MXene* holds a great promise for printable, bendable, flexible, and twistable electronics and coatings—all with tunable electrical, optical (including photonics and plasmonics), mechanical, and electromagnetic shielding properties. Towards this goal, the design and synthesis of *MXene* inks provide a very attractive manufacturing route for flexible *MXetronics*.

The current state-of-the-art *MXene* ink largely involves titanium carbide ($Ti_3C_2T_x$) as the material system and water as solvent material. Within water-based inks, furthermore, inks with ultra-large high aspect ratio *MXene* (lateral size more than 10 µm and predominantly few layers thick *MXene*) versus inks with smaller flake size and smaller aspect ratio (lateral size more than 1 µm and few layers thick *MXene*) have been demonstrated with different performance metrics such as the figure of merits of transparent coating [9]. Although organic solvents such as isopropanol, dimethyl sulfoxide, N, N-dimethylformamide, N-methyl-2-pyrrolidone, propylene carbonate, and ethanol disperse *MXene* well, however, they potentially degrade the physical properties of the ink, among which the electrical conductivity that constitutes one of the most important properties of MXene [10].

The section below focuses on the inkjet printing science and technology of *MXene* conductive inks.

IJP as a state-of-the-art additive manufacturing process

Inkjet printing (IJP), employing a drop-on-demand (DoD) mechanism of individual droplets consisting of materials with nano/micro-particles of interest, is considered as a state-of-the-art printed electronics technique where one can manipulate the drop deposition via an electrical actuation mechanism, thereby provides a powerful method of enabling digital manufacturing. Among the vast number of advantages, the most significant ones are its ability to (a) exploit a wide variety of novel materials; (b) enable high spatial resolution and accuracy in printing; and (c) integrating the process within a hybrid manufacturing platform via automation. Moreover, the simplicity, low-cost and low material use in manufacturing, and parallel processing in enabling seamless pattering consisting of multiple features in a given design make the technique most attractive.

Although IJP has been there for number of other materials such as wide variety of metal nanoparticles (such as silver and copper nanoparticles), various nanowires, fullerenes, and carbon nanotubes for flexible and printed electronics, recently it has been widely adopted for 2D materials such as graphene, and molybdenum disulfide, and so on [11–14]. Therefore, IJP of emerging conductive *MXene* inks will offer a promising manufacturing approach of this novel class of 2D materials in many applications including micro-supercapacitors, sensor electrodes, thin film batteries, flexible electronics, wearable electronics, e-skins, implantable biomedical devices, food safety and packaging in internet of things (IoT) using artificial intelligence [15–18]. Exploiting the tunable and novel properties in 2D layered *MXene* (such as electrical conductivity and other physio-chemical properties) in printed electronics form, will therefore be identified as an attractive avenue that necessitates formulation science of *MXene* conducting inks and their subsequent use in IJP [19]. In recent years, diverse technological innovations have brought significant developments in various printing techniques including screen printing, spray coating, IJP, and extrusion-based three-dimensional (3D) printing [20, 21]. Each technique has its own advantages and disadvantages; however, collectively they have brought a wide number of printed electronics applications in multiple areas of technologies [11, 22–25].

IJP of 2D materials and *MXene*

The first IJP of 2D materials was reported in 2011 by Huang et al., where 2D graphene-based conductive inks were developed for a direct IJP on flexible substrates and was demonstrated in the use of electronic circuits and sensors [26]. After this report, a serious of work has been made on IJP graphene using exfoliated graphene-based conductive inks including our work on graphene aerosol-gel material [27]. The extreme physio-chemical properties of functional graphene materials are each shown to provide many opportunities to fabricate devices with multifunctional features but also possess challenges in device fabrications including manufacturing [28]. The largely explored 2D graphene-based conducting colloidal inks can be mostly influenced by their size, lateral distribution, surface chemistry, functional moieties, aggregation tendency, and dispersion stability [29, 30]. Even though remarkable research progress has been made in graphene and its derived materials in printable ink-making technologies, their tunable conductivity, adhesion to the substrate, printing resolution, and material flexibility in terms of turning them more semiconducting, and so on, need to be carried out before standardizing them for printed electronics [16, 19, 30, 31]. Besides, several other 2D layered materials such as black phosphorus [32], boron nitride [33], *MXene* [34], $MoSe_2$ [35], MoS_2 [36], WS_2 [37], WSe_2 [38], SnS and SnS_2 [39] have also been explored to make conductive inks, which can be efficiently applied in printing industries. However, all these require detailed research investigation.

Transition metal carbides and nitrides, named *MXene*, are a relatively new class of 2D layered materials to which considerable interest has been drawn recently due to their exemplary properties beyond graphene and other 2D materials [40–42]. Generally, a top-down chemical exfoliation approach is widely used to exfoliate 2D *MXene* from a 3D ceramic phase called MAX (M- transition metal, A-group IV element, and X-carbon or nitrogen) [43, 44]. Due to the diverse electronic structure of different transition metal elements, the explored members of the *MXene* family show widely different band structures giving rise to different electronic, chemical, mechanical, optical, and thermal properties [45, 46]. The outstanding functional properties such as electrical (>21,000 S/cm) [47, 48], tunable band gap (0.05–2.87 eV) [18, 49], Young's modulus (502 GPa) [50, 51], optical transmittance (>70%@1000 nm) [52], thermal conductivity (131.2 W/m/K) [53] and electrochemical properties of *MXene* materials make them promising candidate for many applications such as batteries [54], super-capacitor [55], electromagnetic interference shielding [56], thin film transistor [57], optoelectronic devices [58], photo detectors [59], gas sensor [60], molecular recognition element [61], antibacterial [46] and cancer therapy [62]. However, the success of the above applications of *MXene* lies in the large scale, stable manufacturability along with their chemical tailoring process [63, 64]. The beauty of wet chemistry-based exfoliation of *MXene* from corresponding MAX phase materials to make and tailor their slurry-like solutions favorable to additive manufacturing/printing and their functional applications [10, 34]. The Most important beneficial aspect of solution-based exfoliation of *MXene* materials is its effectiveness in dispersing in water and various solvents [65, 66].

Previous studies on formulating printable inks by delaminating various 2D materials along with predefined amounts of appropriate solvents, polymeric binders, and surfactants, require post-processing steps to eliminate the unwanted materials that potentially hinder the original properties of materials [16, 19, 24]. However, recent studies on *MXene* ink formulation reveal the major advantages of additive-free MXene-based conductive inks that could eliminate the post-processing and post-printing steps [34, 67]. Exploring structure-property-relation of *MXene* materials for new applications is still a demanding field regardless of its significant progress in the field. Particularly the ability of *MXene* to form water-based inks is an advantage for eco-friendly printable electronics. Considerable areas of applications of *MXene*-based materials, devices, and systems, in addition, have also forecasted the future promise of *MXene* [10, 22, 68]. Early discovery of acid-based etching and solution processing of *MXene* has provided the recent idea of *MXene* ink synthesis and expanded its possible application to printed electronics of various forms [10, 68–70]. The most reliable IJP method requires essential knowledge in developing printable inks since the higher resolution of printed patterns in the micron range critically requires controlled ink characteristics with very low solid contents, specific rheological properties, printable viscosity, and controlled particle size. To our knowledge, thorough work on the development of *MXene* colloidal ink and the IJP of its fabricated devices for various applications are the widely open fields in *MXene* research. Additionally, understanding and exploring the structure-ink processing-printing-properties roadmap of *MXene* will be essential for the practical realization of this emerging material in the near- and long-term future.

This review provides a salient framework of *MXene* ink formulation specifically for IJP using novel 2D *MXene* materials and their broad practical applications for printed flexible electronic and sensor devices. In addition to that, an outline of various challenges, future perspectives, and outlook of IJP *MXene* inks are presented. The present review is narrated in an interactive form as follows: *MXene* synthesis routes for colloidal suspension formulation, *MXene* IJP and applications, outlook, and conclusions.

MXENE SYNTHESIS ROUTES FOR COLLOIDAL SUSPENSION FORMULATION

Originally *MXene* ($M_{n+1}X_n$) materials were extracted from 3D ceramic MAX phase materials [71]. The compact ceramic MAX phase materials are subjected to react with etchant (fluoride-based etchant) leading to the removal of the Al or Si layer and producing *MXene* (Figure 1a). The etched A-layers are removed from the *MXene* by continuous washing with water. The above two processes (etching and washing with water) provide the inherent formation of hydroxyl (-OH), oxygen (-O), and fluoride (-F) groups, typically as an attachment to the parent *MXene* sheets as shown in Figure 1b. Therefore, often *MXene* is referenced by $M_{n+1}X_nT_x$(T_x = -OH/-F)

[72, 73]. Figure 1 (A and B) shows a schematic diagram of the progress on *MXene* from the MAX phase. Depending on the number of atoms (n = 1, 2, 3, and 4) in M and X elements in each 2D layer, different *MXene* materials could form (Figure 1c) [74]. The most striking properties of *MXene* materials showed a wide range of electrical conductivities (could reach as high as 21,000 S/cm) [75]. Later, different approaches have been applied to prepare *MXene* materials including mild acid and fluoride-free etchants [41, 76, 77].

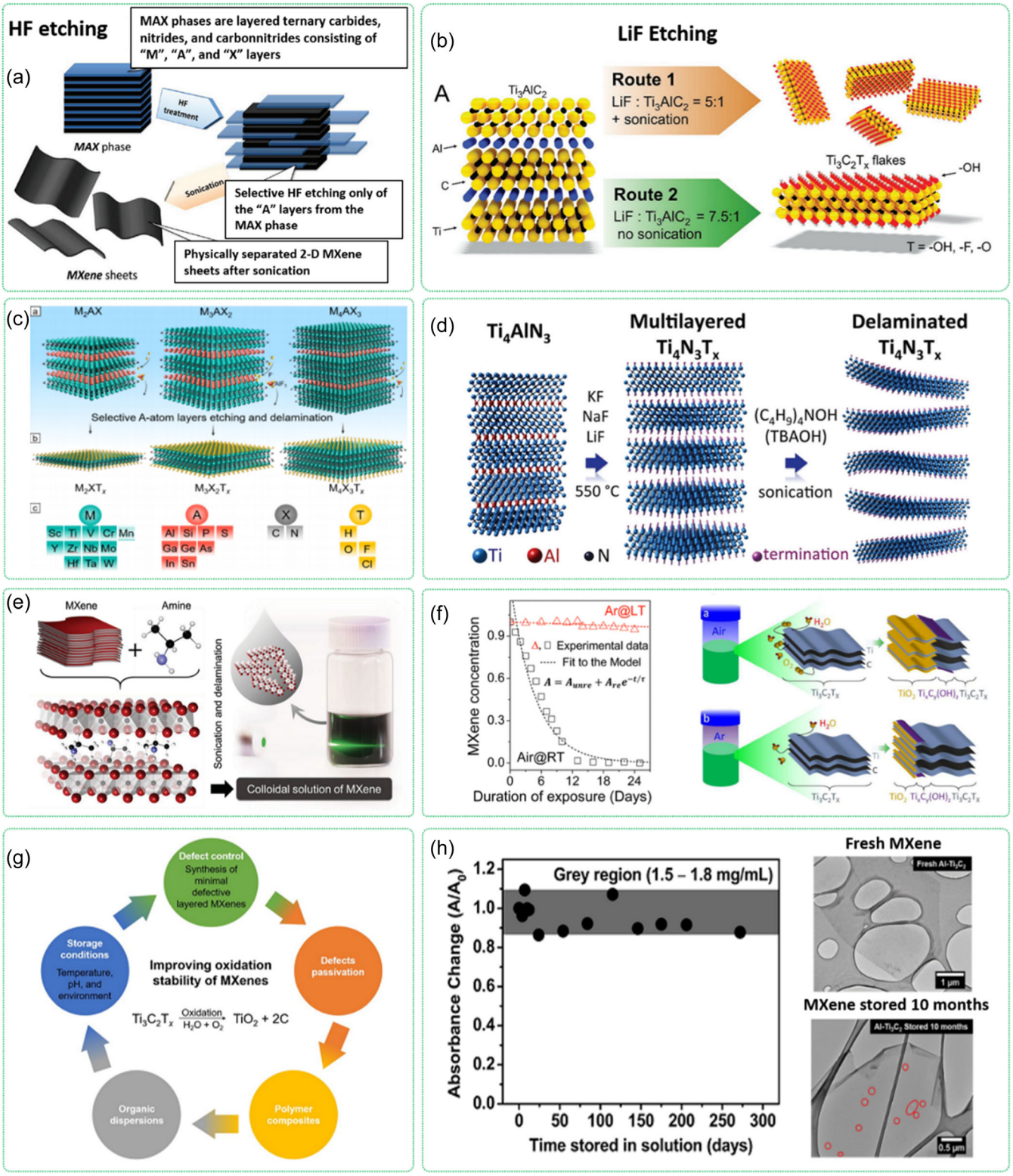

FIGURE 1 (See caption on next page).

The obtained accordion-like morphology contains tightly packed layered structures that still requires post-processing steps such as delamination to obtain a few layer *MXene* [78, 79].

Similar to other 2D materials liquid phase exfoliation (LPE), the primary experimental parameters needed to obtain dispersion are flake thickness and thickness distribution, lateral size and size distribution, surface functionalization, concentration, and solvents [80]. Alternatively, different etching methods with different etchant combinations such as NH_4HF_2 [81], LiF and HCL, Minimum intensive layer delamination (MILD) [82], mixtures of HF and H_2O_2 [83], and Lewis acidic etching [10] were developed [43, 75, 78]. Moreover, several attempts were made to prepare *MXene* materials namely fluoride-free etchant [84], electrochemical exfoliation [85], and bottom-up synthesis by magnetron sputtering [86]. In the later methods, synthesized *MXene* materials possess structural irregularities along with other impurities leading to poor structural stability. The vital factors needed to be considered during chemical exfoliation methods are (i) pre-preparatory acid in a fume hood, (ii) careful addition of MAX into the acid mixtures, (iii) type of MAX phase material chosen (% of MAX phase, mesh size [40–400 µm] [e.g., Figure 1d], and percentage of purity [98%–99.999%]), [72] and (iv) etching parameters (for chosen MAX phase) [87]. Therefore, thorough optimization of etching conditions and subsequent post-processing steps are required to get reliable and reproducible *MXene* materials. Other reaction parameters such as etching concentration, weight ratio of MAX material, reaction time, and etching temperature also play an important role in *MXene* exfoliation. For instance, Ti_3AlC_2 MAX requires 24 ~ 48 h of etching time in HF to remove the Al layer completely [44]. However, Nb_2AlC_2 MAX needs more than 90 h of etching in HF to remove the same Al layer to form $Nb_2C_2T_x$ [88]. Even though there are advantages to different etching methods, the MILD approach is widely used to extract a few layers of *MXene* [41] since it doesn't require post-processing steps such as exfoliation and delamination (Figure 1e) [89] Large-scale synthesis via etching (~50 g of Ti_3AlC_2 MAX phase) was also successfully demonstrated with identical structural and functional properties to small-scale synthesized $Ti_3C_xT_x$ *MXene* [64]. Although high-volume manufacturing of *MXene* is highly sought to bring it for large-scale MXetronics applications, several fundamental bottlenecks need to be addressed. *MXene* synthesis majorly involves the use of strong chemical etchants that create artificial defects in layered assembly specifically forming single atomic Ti vacancies and defect clusters [90–93], which are vulnerable to initiate oxidation.

It has been established that *MXene* oxidizes in water and/or in the presence of atmospheric oxygen conditions followed by the formation of metal oxide nanoparticles that are initiated from edges to inside 2D layers, as shown in Figure 1f [75, 82, 94, 95] There are other factors including defect density, flake size, surface functional groups, dispersing solvents, additives, and binders that are directly involved in the oxidation of *MXene* [75]. Therefore, considerable attention is required (such as structural quality of MAX phase [78], synthesis parameters [43], ultrasonication [96], and post-etching processing [41]) to control the oxidation kinetics of the synthesized *MXene* not only from initial etching experiments but also additional care is needed for storage environment such as temperature, gas atmospheric condition, humidity, pH, and dispersants [94, 97]. Significant research work is in progress for the suppression of oxidation kinetics of colloidal *MXene*. Specifically, storing the *MXene* flakes in an organic dispersant such as ethanol, dimethyl formamide (DMF), N-Methylpyrrolidone (NMP), hexanol, isopropyl alcohol, and chloroform has been shown to delay the formation of TiO_2 nanoparticles unlike their dispersion in water [34, 65–67, 98]. Although effective surface functionalization such as anchoring of organic ligands [97] [99] on the surface, edges, and defective sites of *MXene* layers would passivate the oxidation reaction thereby increasing the stability of the *MXene* materials, it is hard to control in experiments [100]. Chemical grafting of phosphonic acids [101] through interfacial nucleophilic addition, functionalization with di (hydrogenated tallow)benzyl methyl ammonium chloride (DHT) [98] and polydopamine [102], covering the layered surface with antioxidants [99], and addition of ionic liquids [103] in *MXene* colloids favorably suppresses the steric hindrance of water molecules and dissolved oxygen [104]. In addition to that, different approaches to prevent and mitigate the oxidation of *MXene*, the self-life of highly concentrated *MXene* dispersion dramatically increases by making concentrated *MXene* suspension. Interlayer steric shielding in

FIGURE 1 (a) Chemical exfoliation of accordion type 2D *MXene* extracted from 3D MAX phases by HF etching. Adapted with permission from Ref. 73. © 2012 American Chemical Society, (b) Exfoliation of few-layer *MXene* without post-delamination step by using MILD method (LiF and HCl as an etchant solution) to remove aluminum layer from Ti_3AlC_2 MAX phase, Adapted with permission from Ref. 78. © 2016 WILEY-VCH Verlag GmbH & Co. KGaA, Weinheim, (c) Preparation of different MAX phases (M_2AX, M_3AX_2, M_4AX_3) as a source for *MXene* synthesis. Different *MXene* is prepared by selectively removing aluminum (more generally, A-groups) along with the formation of different surface terminations groups. Adapted with permission from Ref. 74. © 2020 Materials Research Society, (d) Synthesis of $Ti_4N_3T_x$ by molten salt treatment. Adapted with permission from Ref. © [71], 2016 The Royal Society of Chemistry, and (e) Intercalation of different external foreign ions/molecules between the individual *MXene* layers to delaminate the individual layers. Adapted with permission from Ref. 89. © 2015 WILEY-VCH Verlag GmbH & Co. KGaA, Weinheim, (f) Stability of colloidal *MXene* in different environments and their degradation (in aqueous solution) in (a) air at room temperature and (b) continuous source for *MXene* degradation induced by the high solubility of oxygen in water during this storage. Adapted with permission from Ref. 95. © 2017 American Chemical Society, (g) Factors controlling oxidation of *MXene* colloidal suspension. Adapted with permission from Ref. 94. © 2021 BioMed Central Ltd., and (h) Stable absorbance of *MXene* suspension stored in water for 300 days, inset figures show TEM images of fresh and stored *MXene* colloidal suspension for 10 months. Adapted with permission from Ref. 72. © 2021 American Chemical Society.

concentrated *MXene* colloids is less likely to allow water molecules to enter between *MXene* sheets and decelerate their rate of oxidation.

MXENE IJP AND APPLICATIONS

MXene IJP parameters

IJP technology is identified as a breakthrough additive manufacturing technique for attaining high-resolution printing to design and manufacture printed electronics, including flexible, bendable, stretchable, and conformal electronics. IJP affords several advantages compared to other printing techniques (Figure 2a) namely, contactless printing, higher resolution down to sub-ten micrometer feature size, printing computability with a wide variety of platforms, low cost and material efficiency, simplified printing process with predefined ink conditions and ease of integration with different substrates [16, 24, 25]. Compared with conventional silicon manufacturing approaches that require higher-end fabrication tools and extended fabrication processes. IJP employs a three-step simplified process: Ink formation, printing, and post-printing treatment.

The basic process behind the IJP is the jetting of ink material from the nozzle with the desired size followed by impaction and deposition on the substrate plate in a controlled manner. Based on the printing process, two jetting mechanisms were used in IJP such as continuous inkjet (CIJ) and drop on demand (DoD) [105]. CIJ is the first printing technology started in the early 1950s and is widely used in industrial purposes such as for label making. CIJ has the ability to make a continuous stream of ink that precisely controls the ink droplets making it possible to write on a desired substrate. Whereas, the DoD system (Figure 2b) is widely used to print functional materials since the printing mechanism allows discrete ink droplets ejected only when required and also its ability to control the droplet size (20–50 μm), which enhances the resolution of printed patterns.

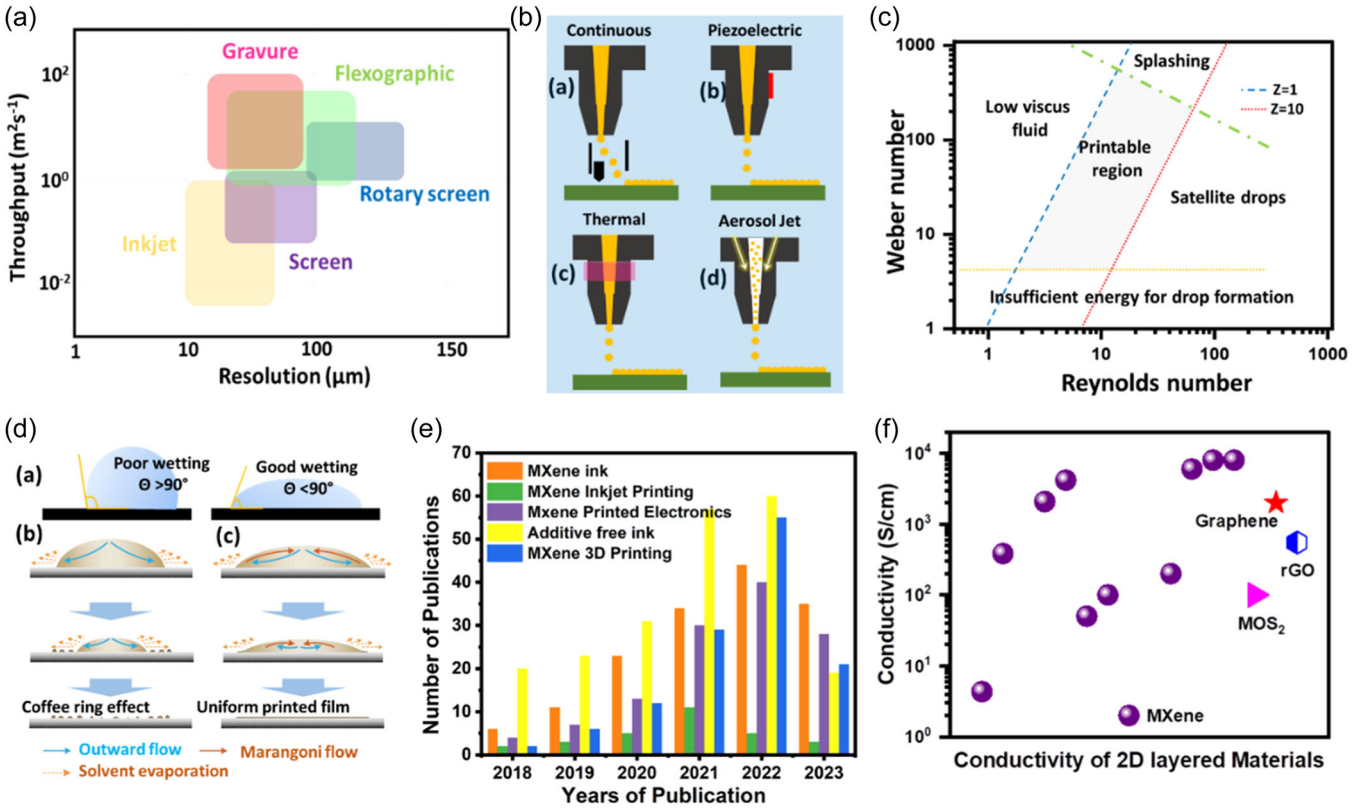

FIGURE 2 (a) Comparison analysis of printing throughput and attainable printing resolution for various printing approaches. Reproduced with permission from Ref. 15. © 2018 The Royal Society of Chemistry, (b) Schematic diagram of different mechanism-based IJP (a) continuous, (b) Piezoelectric, (c) thermal, and (d) aerosol IJP, reproduced with permission from Ref. 105. © 2019 The Royal Society of Chemistry, (c) Ink rheological properties and its relation to printable conditions, showing region of fluidic properties with dimensionless parameter (Z). Reproduced with permission from Ref. 113. © 2010 by Annual Review, (d) Schematic illustration of substrate-ink interactions with (a) poor and good surface wetting, (b) typical evaporation profile on good surface wetting and formation of the coffee right effect due to higher rate of ink evaporation at the edges and outward flow from the droplet center, and (c) schematic representation of the Marangoni effect of solute by controlling ink rheological properties or by addition of solvents to increase inward Marangoni flow. This could evenly distribute the ink with controlled ink evaporation for the formation of homogenous IJP films. Reproduced with permission from Ref. 32. © 2017 Springer Nature Limited, (e) The research trend on topics such as "*MXene* ink", "*MXene* inkjet printing", "*MXene* printed electronics", "Additive-free ink" and "*MXene* 3D Printing" collected from the past 6 years of publications (source, web of Science), and (f) Demonstrated electrical conductivity of different *MXene* inks to-date compared with a state-of-the-art other 2D materials.

[106]. The controllable ink droplet is achieved via thermal, piezoelectric, and aerosolization mechanisms (Figure 2b) based on the system chosen. Different tunable IJP parameters result in customizable printing patterns with tunable resolution. However, the quality and physical parameters of formulated ink and the surface on which the printing is desired will strongly rely on the quality of discrete droplet formation (without satellite drops), continuous printing, resolution of printed patterns, and ink-substrate interactions [107, 108]. Solvent-based ink formulation is widely applied to make IJP ink with proper ink rheology and viscosity. In addition, appropriate binders are employed along with the solvent to achieve stable dispersion and to tailor the ink rheology and viscosity, however, additives/binders have dramatic effects on the printed films and their properties such as electrical conductivity and quality of printed film assembly [109, 110].

Ideally, basic processes involved in IJP such as ink synthesis, droplet formation, stable ink jetting, and satellite droplet formation are determined by dimensional physical parameters such as the Weber number (W_e), the Reynold number (Re), and the Ohnesorge (*Oh*) number as shown in Equations (1–3) [111, 112].

$$W_e = \frac{\upsilon^2 \rho \alpha}{\gamma} \tag{1}$$

$$R_e = \frac{\upsilon \rho \alpha}{\eta} \tag{2}$$

$$Oh = \frac{\sqrt{W_e}}{R_e} = \frac{\eta}{\sqrt{(\gamma \rho \alpha)}} \tag{3}$$

Where, υ, γ, ρ, α and η are droplet velocity (m/s), ink surface tension (mN/m), ink density (g/cm^3), diameter of nozzle (μm), and ink viscosity (mPa-s), respectively. The reciprocal of the *Oh* gives the dimensionless quantity Z, which provides the information to evaluate the figure of merit of printing with accepted values of $1 < Z < 10$ [113]. For smaller Z values, the ink must be highly viscous to prevent droplet splitting, whereas Z above 10 leads to the formation of unwanted satellite drops. In addition, W_e should be above 4, for the new droplets possess threshold energy to overcome ejection energy barrier [114]. By taking into account different parameters involved in IJP, a 2D Cartesian plot is given in Figure 2c which depicts the IJP parameters for effective printing [32]. Moreover, high-resolution printing can be achieved by formulating high-quality ink and deposition behavior onto the substrate platform, and substrate pretreatment. Concerning the nature of substrate material implementing an appropriate choice of solvent additive or dispersant, surface pretreatment, or coating on a substrate with low surface energy material could result in inward Marangoni flows to get uniform printed patterns without the "coffee ring effect" [114–116] as given in Figure 2d.

Based on the above discussed IJP process parameters, there are several stringent conditions for the formulation of *MXene*-based inks. For example, the IJP technique needs inks with low viscosity (typical range 5–20 cPa) and suitable surface tension for continuous jetting without satellite drop formation. This requires inks with lesser concentrations of materials with higher solvents/dispersants compared with other printable inks. Therefore it enables printing thinner layer (~10 nm thickness) of printed material compared to screen printing [15, 29]. Currently, most of the *MXene* IJP printable inks use solvent-based medium to suspend the *MXene* primarily because they tune the dimensionless parameters (Z) as well as maintaining the stability of printed structure even though *MXene* dispersion is primarily exfoliated in water medium. Therefore, the solvent exchange procedure is desirable for stable IJP *MXene* ink formulation. For example, DMF, NMP, dimethyl sulfoxide (DMSO), and isopropyl amine (iPA) solvents were used for making IJP *MXene* ink in addition to water-based ink. The intrinsic hydrophilic nature of *MXene* flakes tends to form stable ink suspensions in water and selective solvents without the addition of a binder. Recent reports elucidate that the development of *MXene*-based additive-free and highly conducting inks have the potential for various IJP-based device fabrication for various applications (Figure 2e, f) [34, 67, 104]. Therefore, it is interesting to discuss different IJP *MXene* functional devices and their potential application areas (see Table 1).

Applications of IJP *MXene*

Below we describe some of the most important applications of IJP *MXene* that possess potential future interest including those in flexible, bendable, and twistable platform.

Application in printed electronics, bioelectronics, and EMI shielding

IJP *MXene* has recently shown several promising applications such as printed micro-supercapacitors (including transparent supercapacitors), wearable textile energy storage devices, electromagnetic interference shielding, biosensing, and ultrafast photonic devices such as saturable absorbers (see Table 1). The first report on IJP was on self-assembled *MXene* electrodes by Vural et al in 2018 [117], were multi-model properties such as LED circuit fabrication, stimuli response, and electromagnetic interference shielding (EMI) shielding performance were discussed. The solvent-exchanged *MXene*/DMSO inks showed higher Z values around 27.5, which were further tuned by the addition of synthetic polypeptide protein (0.95 mg/ml) capable of making suitable printable inks at a viscosity of 3.4 cP and surface tension of 40 mN/m with *MXene* concentrations of 2.25 mg/ml (Figure 3a–c). The bio-macromolecular structure favors forming and maintaining a low viscosity *MXene* inks, improving the substrate adhesion properties thereby helping free off the coffee ring effect in printed patterns. Besides, the synthesis of bio-additive amino acid-based *MXene* inks is adequate for IJP on various substrates such as glass, PET, PMMA, and PDMS without pretreatment, whereas PMMA has strong surface sticking affinity with *MXene* ink due to dissolution of DMSO. Their experimental observation on different IJP

TABLE 1 Summary of *MXene* synthesis, ink formulation, rheological properties of inks with functional applications.

Etching Conditions	Dispersant	Binder/ Additive	Ink rheological properties	Substrate	Applications	Published Year
LiF+ HCl	DMSO	Polypeptide	Z −21.3γ − 40 η − 3.4	glass, PET, PDMS, PMMA,	LED, Response to Humid, and EMI shielding	2018 [117]
LiF+ HCl	Water	Graphene+ Nafion	ND	Un treated Glass, and gold foil,	Electrochemical H_2O_2 sensing	2018 [118]
LiF+ HCl MILD	DMSO, NMP, DMF,	NANANA	$Z_{Ethanol}$ − $2.6Z_{DMSO}$ − $2.5Z_{NMP}$ − 2.2γ − 22.1 to 43.5η − 7.3 to 12.8	AlO_x-coated PET, not fit for Glass and PI	IJP micro-supercapacitors	2019 [67]
HF	IPA	NA	Z −8.3γ − 23η − 2.4	silica glass, SiO_2/Si, fiber, and PET, and gold mirror	Ultrafast Photonic Devices- Saturable Absorber IJP	2019 [119]
LiF+ HCl (MILD)	Water	Sodium ascorbate	Z − 19.41γ − 46 η − 1.7	photopaper	IJP micro-supercapacitor	2020 [120]
HF+HCl (LiF- Post Delamination)	Water	Saponin	Z − 15.6γ − 64η − 1.5	glass, paper, PEDOT:PSS film	Multimodel cutaneous biosensing	2020 [121]
HF+HCl (LiF- Post Delamination)	Water	NA	Z − 19.9 to 18.9γ − 76.5 to 68.8η − 5.1 to 1.7	textile	Energy storage Textile	2020 [34]
HF+HCl (LiF- Post Delamination)	Water	NA	Z − 30γ − 80.3η − 4	Kapton, Silicon,	*MXene*-Graphene heterostructures	2021 [122]
LiF+ HCl (MILD)	Water + NMP	NA	Z − 7.8 to 15.8, γ − 47.2, η − 2.3 to 4.6	PET adhesive paper,	All printed Transparent supercapacitor	2021 [123]
LiF+HCl	NMP	Graphene	Z − 1.9γ − 46.2η − 18.1	PET	IJP composite films for supercapacitor electrodes	2022 [124]

Note: Surface Tension (γ, mN/m,), Viscosity (η, mPa·s), Inverse Ohnesorge Number (Z), NA – No additive, ND - Not determined.

parameters reveals that synthesized *MXene* inks can reach higher resolution printing in the range of 40–150 µm that can further be tunable by varying physical characteristics of the inks. However, the presence of such additive molecules will have an observable impact on the electrical conductivity of layer-by-layer printed structure to a reduced value that yet needs to be addressed (e.g., the conductivity of 1080 ± 175 S/cm with an average printed pattern thickness of 2.25 µm) [117]. Nevertheless, the above IJP *MXene* flexible patterns on PET films give light-emitting diodes (LED) characteristics interesting for future printed electronics. Moreover, the low resistive IJP *MXene* films provide efficient EMI shielding performance with an attenuating effectiveness of 50 dB (Figure 3d) at a film thickness of 1.35 µm, which is far superior to the ones used in commercial EMI shielding materials (~20 dB). The EMI shield applications have also been effectively conducted in different humid conditions.

Implementation of the IJP *MXene* pattern in biological applications could open new avenues in bio-electronic applications. Zheng and their research group [118] have developed an IJP *MXene*-Graphene electrode for the electrochemical detection of hydrogen peroxide (H_2O_2), a fundamental element involved in glucose sensing. The MAX phases were chemically treated with mixtures of LiF and HCl resulting in the formation of a few layered *MXene*. The few-layered *MXene* was ball milled with graphene oxide (GO) suspension in the presence of Nafion binder resulting in the formation of water-based *MXene*-GO-Nafion ink suspension (particle size ≈ 100 nm), that were subsequently used for IJP on UV pretreated glass and gold foils. The IJP sensor electrodes demonstrated enhanced electrochemical catalytic oxidation and reduction reaction along with good surface adhesion. They were also functionalized with hemoglobin (*Hb*) to activate electrodes for selective electrochemical sensing of glucose. The applied differential pulsed voltammetry technique using *Hb* functionalized *MXene*-GO sensor electrodes could detect H_2O_2 molecules in the detection range of 2 µM to 1 mM with a detection limit of about 1.95 µM. Furthermore, the real biological blood samples test results obtained from the *MXene* sensor resulting in only a 4.48% standard deviation shows their potential for low-cost printed *MXene* bioelectronics.

Application in printed supercapacitors

MXene is most widely used for its superior properties in energy storage in the form of supercapacitors. As such printed *MXene* supercapacitors possess very promising applications for printed flexible *MXetronics* [18]. Adding functional binder molecules preferably enriches the rheological properties of ink suspension aiding them

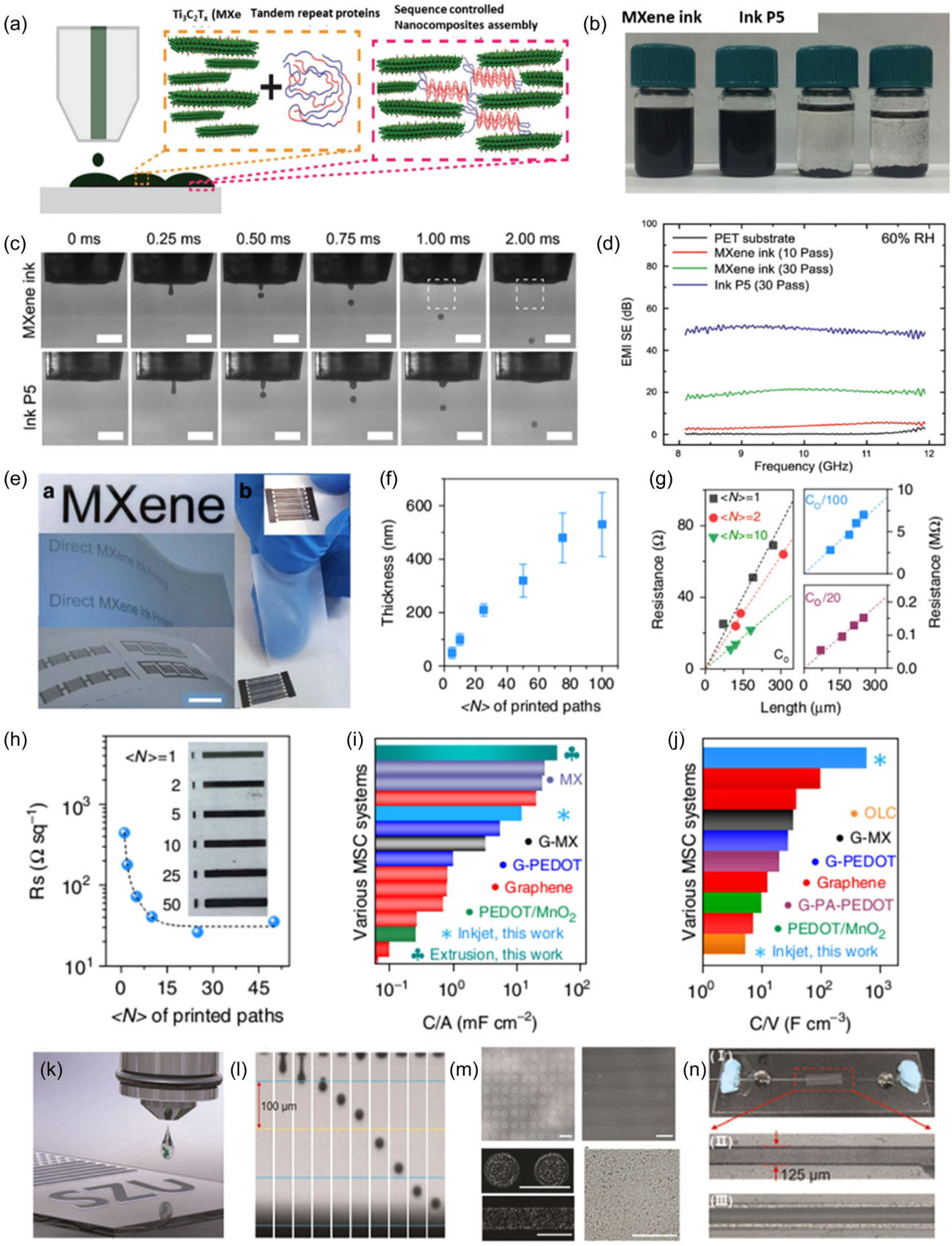

FIGURE 3 (See caption on next page).

for reliable IJP printing. However, the addition of external agents into the ink suspensions requires a post-printing procedure for removal. Even the presence of molecular fractions of residue molecules complicates the final device performance. Alternatively, water-dispersible *MXene* can be solvent exchanged for the desired solvents to form additive-free printable *MXene* inks. Even though *MXene* has been identified as a great material in energy applications, significant challenges need to be addressed. Specifically, conventional polymer-based stabilized ink requires post-thermal treatment which is not compatible with *MXene* due to thermally induced oxidation leading to degradation. Moreover, commonly used low boiling point solvents tend to precipitate the *MXene* layers, hence limiting the synthesis of highly concentrated ink suspension. To overcome these practical difficulties in preparing the *MXene* IJP, Zhang et al., [67] came up with the idea of making an additive-free and binary solvent *MXene* ink synthesis protocol that eliminates ink pre- and post-processing steps. Initially, widely used MILD exfoliation procedures were adopted to prepare the *MXene* wet slurry, which is subjected to manual hand shaking or controlled bath sonication followed by centrifugation leading to extraction of a few-layer *MXene* suspension. The extracted *MXene* was re-suspended in different organic solvents such as NMP, DMSO, DMF, and ethanol to attain stable colloidal suspensions suitable to store in ice-cold conditions to prevent oxidation (self-life of more than 12 months except in DMSO). The dimensionless quantity (Z) of the prepared *MXene* inks was individually calculated for different inks and is within the range 2.2 (NMP), 2.5 (DMSO), and 2.6 (Ethanol) for IJP purposes. The AlO_x-coated polyethylene terephthalate (PET) substrates were used for effective IJP for different *MXene* ink suspensions to overcome substrate wetting issues, and the resolution of printed patterns was in the range between 50 and 130 µm. By tuning additive-free *MXene* inks, the printed patterns show good mechanical flexibility over 1000 bending cycles and retain uniform printing assembly, however, conductivity loss of up to 80% from its initial values (2770 S/cm) after 6 months of ambient exposure. In addition to that, the *MXene* IJP patterns show line resistivity in the range of 0.12–0.27 Ω/µm for different printing passes, which opens the door for applications in flexible printed analog circuits (Figure 3e–h). The charge storage performance of *MXene* IJP electrodes was analyzed in the presence of a standard PVA/H_2SO_4 electrolyte, which showed a pseudo-capacitive response with a scan rate capability of 1 V/s. Remarkably, the IJP *MXene* supercapacitors show higher volumetric capacitance of about 562 F/cm^3 compared to printed graphene micro supercapacitors (~100 F/cm^3) (Figure 3i, j).

Application in printed photonic devices

In a different approach, Jiang et al., [119] reported the IJP *MXene* microscale devices for integrated broadband ultrafast photonic applications (Figure 3k–n). In their work, low boiling point, less toxic, and binder-free *MXene* inks were formulated using IPA as a dispersant. Traditional HF-based exfoliation methods were applied to obtain accordion-like morphology of stacked *MXene* layers, which were further subjected to controlled sonication in IPA solvent to extract a few layers of *MXene* (2 mg/ml). The particle size and thickness of the extracted few layers of *MXene* is in the range of 21.5 ± 7.6 nm and 3.7 ± 0.7 nm, respectively which are desired size for IJP nozzles to print. The calculated dimensionless quantity (Z) of *MXene*-IPA inks was about 8.3, which was adequate for IJP. In addition to that, the synthesized *MXene* inks had a 3-month self-life under refrigerated conditions. Remarkably, IJP functional devices were printed in different substrates such as silica glass, SiO_2/Si wafer, side-polished fiber, flexible and transparent PET film, and gold mirror without prior surface coating. By tuning IJP parameters, different patterns were reported (Figure 3k–m). Furthermore, by choosing a suitable IJP approach for *MXene* inks, different saturable absorbers (Figure 3n) were constructed in different substrate platforms. Experimental results depicted that the output laser performance of the solid-state Q-switched lasers is superior compared with various 2D material-based saturable absorbers. Demonstrated printed *MXene* saturable absorber coating paves for *MXene*-based advanced photonic devices.

Application in printed micro-batteries

The development of IJP microelectrodes is an emerging field in micro-batteries and -supercapacitors due to their fine tunable electrode components that power microelectronic devices and portable sensors. In this connection, Wu et al., [120] solved the dual issues of *MXene* oxidation followed by charge cycle instability and

FIGURE 3 (a) schematic representation of the polypeptide protein-mediated assembly of *MXene* sheets, (b) subsequently formulated *MXene* inks with different loading of bio-macromolecules in DMSO solvents, (c) comparative stroboscopic pictorial images of pure *MXene* and protein-mediated *MXene* ink droplet formation and jetting from the nozzle, (d) EMI shielding performance of IJP *MXene* on PET substrate at 60% RH. Reproduced with permission from Ref. 117. © 2018 WILEY-VCH Verlag GmbH & Co. KGaA, Weinheim, (e) Additive free *MXene* IJP on AlO_x coated PET (direct *MXene* Ink Printing) in the form of micro-supercapacitors, (f) thickness of printed *MXene* with printing pass number, (g) variation in resistance of printed layer length for different printing passes, (h) sheet resistance of the printed lines with different printing passes, (i–j) areal capacitance (C/A) and volumetric capacitance (C/V) comparison of *MXene* IJP compared with previously reported supercapacitors with layered and other nanostructured materials. Reproduced with permission from Ref. 67. © 2019 Springer Nature Limited, (k–n) schematic of the *MXene* ink jetting from a printing nozzle; sequence and formation of printing droplets (without satellite formation) as observed in a stroboscopic camera; printing of uniform circular and line patterns with higher resolution (scale bar 100 µm) and side polished fiber saturable absorber, with the optical images taken from a side-polished IPJ *MXene*. Reproduced with permission from Ref. 119. © 2019 Springer Nature Limited.

used IJP *MXene* patterns for micro-supercapacitor applications. The different water-soluble binders such as sodium ascorbate (SA), sodium citrate, sodium oxalate, and sodium phosphate were used as oxidation inhibitors to prepare *MXene* ink suspension by continuous sonication and centrifugation process. Of the above different considered additive materials, the compound with SA ligands showed increased lifetime (>80 days) of *MXene* suspensions along with reduction of lateral size of the *MXene* layers <200 nm due to strong affinity of enediol compounds towards surface exposed under coordinated Ti atoms present at the edges of *MXene* layers. Fractional amounts of propylene glycol and Triton X-100 were added to attain a printable *MXene* ink (Z-19.4) with a dynamic viscosity of 1–1.7 cP preferable for IJP. The IJP *MXene* microelectrodes with a thickness of 1.5 µm were fabricated without Marangoni flow. The printed microelectrodes showed conductivity of about 119 S/cm, which remains 78% intact after 20 days of exposure to atmospheric conditions. Further, the fabricated PVA/H_2SO_4-SA-*MXene* supercapacitor assembly possessed 94.7% of the initial capacitance after 4000 charge/discharge cycles at a current density of 1 A/g.

Application in printed biosensors and wearable hybrid biosensors

The IJP technique offers a straightforward route for the low-cost, and large-scale production of wearable biosensors. Interesting applications of IJP *MXene* on multimodel cutaneous biosensing applications (Figure 4a) have been reported by Saleh et at. [121] In their report, printable inks were prepared with simple mixing of predefined concentrations of *MXene* (2 mg/ml) with cationic, anionic, and nonionic (saponin) solvents by vortex mixing. The printability of synthesized inks accessed from the dimensionless parameter (Z) is about 15.6 with a viscosity of 1.5 cP and high surface tension of 64 mN/m. The ink rheological parameters of printable inks (Z limiting values) were optimized for different surfactant/additive concentrations. Out of different experimental conditions, saponin showed printable ink suspension along with higher conductivity of about (831.87 ± 76.06 S/cm). The synthesized *MXene* aqueous inks were printed on free-standing polymer flexible substrates, glass, and paper with higher adherence. Experimental observation reveals that saponins were predominantly attached to the surface of printed *MXene* layers thereby helping adhesion. *MXene* inks were printed on flexible conducting polymer substrates that are skin adherent and could sense the electrocardiography (ECG) signals with a high signal-to-noise ratio (7.1) at a device self-life of 50 days in ambient conditions. The obtained air-stable, reusable, gel-free application of IJP *MXene* electrodes could be interesting in future wearable biomedical applications. Further, the IJP *MXene* electrodes integrated with ion (Na^+) selective membrane showed reliable performance in detecting human sweat with a sensitivity of 40 mV per decade. In addition to that antibody functionalied IJP *MXene* electrodes showed outstanding performance for the detection of cytokine protein (IFNγ) molecules in aqueous samples at a sensitivity of 3.9 mV per decade. These results demonstrate the wide applicability of IJP *MXene* in biomedical applications.

Next-generation wearable electronics and energy devices require flexible sensor electrodes, which need to be prepared by different approaches. Printing technology has enabled new pathways for creating and using novel conducting ink-based materials and devices. For example, conductive textiles are salient in flexible, wearable electronic industries. In this connection, Uzum et al., [34] reported additive-free aqueous *MXene* inks for thermal IJP on textiles for energy applications (Figure 4b, c). A newly adopted HCl and HF-based etching approach was used to prepare the stacked *MXene* layers which were further delaminated with LiCl salt by continuous stirring, sonication, and centrifuge-assisted extractions. Finally, extracted Li-free large lateral *MXene* flakes were cut into smaller sizes to avoid clogging of nozzle during the IJP process. The general approach to formulate printable additive-free *MXene* inks with tunable viscosities was demonstrated by controlling structural features of the exfoliated *MXene* materials such as concentrations (18–24 mg/ml), lateral flake size (2 µm, and 350 nm), flake thickness for subsequent application in printing on wide variety of substrates (Figure 4c). The dimensionless printing prerequisite parameter (Z) for different ink suspensions were in the range between 19.9 and 18.9 depending on ink rheology. The easy wettability of porous substrate specifically hydrophilic cotton-based textiles can accelerate ink evaporation rates due to the higher surface area of cotton compared to conventional flexible substrates. The characteristic features of the IJP *MXene* patterns in textile substrates reviewed over 6 months under ambient exposure conditions showed almost intact structures (17.6% increase in resistance) with a small fraction of oxidation. Finally, the *MXene* IJP textile micro supercapacitor demonstrating excellent areal capacitance (294.3 mF/cm^2 at 2 mV/s), exceeded previously reported printed *MXene*-based and other 2D-materials based micro supercapacitors. The printed micro supercapacitor exhibited high energy and power densities of 12.36–4.46 µWh/cm^2 and 0.16–0.58 mW/cm^2, respectively. The developed strategy for direct printing of *MXene* ink materials on the textile substrates combines manufacturing processes and integration of this new class of materials and their electronics up to the textile platform.

Application in printed hybrid *MXene* with other materials

Futuristic development of IJP technology to make controlled 2D layered heterostructure using *MXene* and graphene inks was demonstrated by Wang et al., [122]. Two different water-dispersed *MXene* and graphene inks were prepared individually. Under IJP conditions, the corresponding inks were printed onto a Kapton substrate with layer-by-layer assembly to make all IJP micro-supercapacitors. A conventional chemical exfoliation method was applied to prepare water-based *MXene* suspension with different tunable ink properties with surface tension and viscosity of about 80.3 mN/m and 1.4 cPa and the measured dimensionless quantity

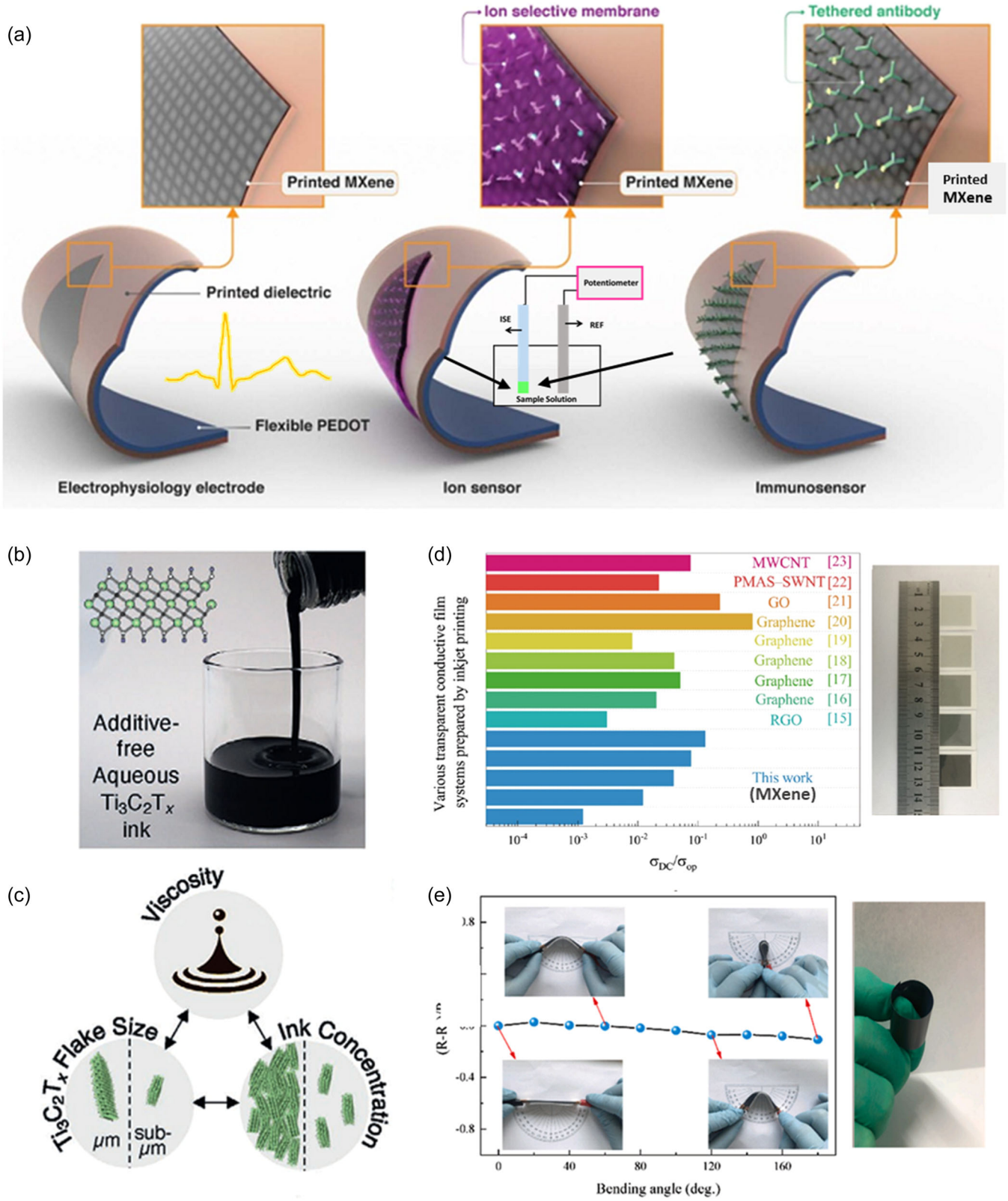

FIGURE 4 (See caption on next page).

(Z) was about 30. Their experimental observations and previous experimental findings reveal that additive-free water-based *MXene* inks show stable printing behaviors without satellite drop formation irrespective of theoretical values $1 < Z < 10$. However, the possibility of getting uniform printed patterns from the *MXene* inks can be achieved from the inherent structural features along with an attachment of different functional groups. Different patterns of the *MXene* electrodes were IJP in a polyimide substrate with pre-optimized printing conditions. The high ionic conductivity and insulating behavior of hydrated graphene oxide nanosheets were used to construct solid-state electrolytes and separators during micro supercapacitor fabrications. The hydrated graphene oxides with Triton X-100 inks served as a source to deliver ions for ionic conductivity by the hydrolysis of functional groups. The clear boundary space between the *MXene* electrodes and graphene electrolyte elucidates well-defined spatial separation without short-circuit. The sandwiched supercapacitors with *MXene*-graphene showed specific areal capacitance up to 9.8 mF/cm^2 at a current density of 40 $\mu A/cm^2$ due to improved ionic conductivity provided by the graphene oxide-Triton X-100. Further, detailed experimental observation suggested different device-printed architectures to improve their area capacitance.

Follow-up studies with different applications of next-generation transparent supercapacitors using IJP *MXene* electrodes were reported by Wen et al., [123] In their report low cost, large area, and rapid preparation of *MXene* transparent patterns on the flexible substrates have been demonstrated for transparent all printed supercapacitors. The size of the final exfoliated *MXene* in the suspension was in the range of 100–350 nm appropriate for jetting in the printer nozzle without clogging. The controlled tuning of NMP concentration in the water-dispersed *MXene* inks (1.3–13.3 mg/ml) favorably makes the ink suspension printable without clogging, satellite drops formation, and more importantly impedes the Marangoni effect. The formulated *MXene* ink suspension maintains uniform dispersion with a high self-life of about 1 month stored in ice-cold condition. The reported inverse of Ohnesorge number (Z) from their formulated *MXene* ink was in the range of 7.8–15.8 with measured surface tension and viscosity of 2.3–4.6 cP and 47.2 mN/m, respectively. Furthermore, the measured acute contact angle of synthesized *MXene* onto the PET substrate indicates the matching of surface tensions between inks and substrate material enhancing wettability. Measured optoelectronic properties reveal that printed *MXene* films achieved lower sheet resistance and optical transmittance of about 1.47 ± 0.1 kΩ/sq and 87%–24%, respectively. This corresponds to a figure of merit (calculated from the ratio of electronic to optical conductivity) of about ~0.0012–0.13 (Figure 4d), providing interesting future potential in printed transparent coating applications. The fabricated printed *MXene* films employed as transparent conductors and active electrodes for energy storage devices (areal capacitance of 192 $\mu F\ cm^{-2}$) surpassed the performance of previously reported graphene and SWCNT-based transparent electrodes. In addition to that transparent supercapacitors retain 100.8% of the initial capacitance values after 180° bending results for future wearable electronic and energy storage devices. The reported performance was comparatively superior compared with previously reported materials which are fabricated in different materials.

In another interesting study, Ma et al., [125] reported micro supercapacitor applications of IJP *MXene*, where poly(3,4-ethylenedioxythiophene): poly(styrenesulfonic acid), called PH1000, was used as a nontoxic solvent for making highly stable *MXene* ink without restacking of *MXene*. In their work, *MXene* was exfoliated from the MILD method and the stable printable conductive ink was prepared by adding 3.3 wt% of PH1000. The role of PH1000 was explained by increased interlayer interactions between the *MXene* layers thereby creating more conducting tunnels for charge transfer. The calculated dimensionless parameter (Z) values of their synthesized ink show 1.81 which was suitable for IJP. Their experimental observation revealed a higher volumetric capacitance of 754 $F\ cm^{-3}$ for the fabricated microsupercapacitors along with a remarkable energy density of 9.4 $mWh\ cm^{-3}$ which is comparably higher than previously reported IJP microsupercapacitors. Moreover, they demonstrated an integrated IJP micro supercapacitor capable of self-powdered operation of a temperature sensor with ≈2% response while exhibiting good mechanical resilience under various bending cycles.

The alternative approach for reducing the restacking of *MXene* layers within the ink environment can be made by the successful mixing of external nanosheets such as graphene sheets. This strategy to develop printable composite inks could pave the way for additive manufacturing of energy devices. Recently, IJP *MXene*/graphene nanocomposite flexible (Figure 4e) electrodes have been fabricated and its electrochemical energy storage application was demonstrated

FIGURE 4 (a) Functionalized IJP *MXene* sensing electrodes on PEDOT substrates were used in electrophysiology monitoring with sodium ion detection and human immunosensor fabrications shown. Reproduced with permission from Ref. 121. © 2020 Published by IOP Publishing Ltd. (b–c) Digital photographs of additive-free *MXene* ink suspension with different concentrations of *MXene* flakes of different lateral sizes. Key components such as flake size, concentration, and viscosity involved in *MXene-based additive*-free ink synthesis are needed to control the ink rheological properties within the dimensionless physical parameters ($1 < Z < 20$). Reproduced with permission from Ref. 34. © 2020 2020 Wiley-VCH GmbH, (d) Comparison of a figure of merit (the ratio of electronic to optical conductivity) of IJP *MXene* with carbon nanotubes, graphene, and reduced graphene oxides. The figure to the right shows samples with varying optical transparencies. Adapted with permission from Ref. 123. © 2021 American Chemical Society, and E. Mechanical stability of IJP *MXene*-graphene nanocomposite inks printed onto the PET substrate with negligible change in the printed electrode resistance, the right image shows the photograph of bendability of *MXene*-based IJP patterns. Reproduced with permission from Ref. 125. © 2022 Elsevier.

by Wen et al., [124] The objective of their work was to find an alternative way to mitigate the self-stacking effect of *MXene* which was addressed by using graphene sheets for composite ink formulation and subsequent printing. The formation of nanocomposite ink showed good stability in the dispersion even after 1 month of storage, showing the benefits of graphene as an additive. Importantly, the decreased sheet resistance upon increasing the graphene loading was explained by increased contact junction resistance between the *MXene* and graphene layers. The closely overlapped *MXene*/graphene nanocomposites printed patterns showed decreasing sheet resistance with increasing the number of printing passes along with excellent mechanical flexibility retention of 80% of the initial value after 100 bending cycles (Figure 4e). Electrochemical anlaysis concludes that the IJP *MXene* with lower graphene additive exhibits excellent stability with 89% resistance retention at a 180° bending angle, the high volumetric capacitance of 183.5 F/cm^3 at a scanning speed of 5 mV/s, and long cycle life with 75% capacitance retention after 3000 charge-discharge cycles. The early work on printable *MXene* composite inks and their electrochemical performance is an important area of research and development for the design and manufacturing of advanced flexible electronic and energy storage devices.

In another study, Gibertini et al., [126] reported an all-IJP *MXene* electrochemical capacitor on the textile surface for wearable energy storage applications, called Textronic, which could have many practical applications. *MXene* source material was prepared by selective etching of the Al layer from MAX by adopting the MILD method. Ball milling and sonication of *MXene* with sodium ascorbate followed by centrifugation process results in controlled size reduction of *MXene* suspension. The desired amount of lithium dodecyl sulfate was added to make the *MXene* ready-to-use ink (Z = 11.8) at an *MXene* concentration of ~1.5 wt%. Similarly, by proper mixing of LiCl, ethylene glycol, acrylamide, and N, N'-Methylenebisacrylamide, and photoinitiator tend to form printable electrolyte precursor (Z = 4.5). By adopting the IJP approach, both *MXene* ink and the electrolyte were printed onto the thermoplastic polyurethane-coated textile fabric to design a symmetrical capacitor. The all-printed-textile-based fabric showed an areal capacitance of 0.89 mF cm^{-2} over 2000 cycles. In addition, the array of IJP symmetric capacitors could serve as an energy storage and micro-power source in this novel platform.

IJP *MXene* micro supercapacitors with higher energy densities are in continual demand such as the one reported recently by Wang et al., [127]. Printable inks were prepared by mixing *MXene* (20 mg/ml), sodium alginate (1 mg/ml), and divalent iron ions (5 mg/ml) followed by sonication and stirring. The selected Fe^{2+} and sodium alginate not only provide a compact 3D structure for ion storage and formation of the conductive network but also provide beneficial ways to prevent the oxidation of *MXene* by forming hydrogen and covalent bonding between the *MXene* nanosheet, SA, and Fe^{2+}. Additionally, sodium alginate molecules provide an effective remedy for *MXene* restacking. Their prepared *MXene*/SA-Fe ink provides high conductivity, tunable viscosity, amazing printability, and long-term stability, critical characteristic features to fabricate mechanically and electrochemically stable microelectrodes. The IJP micro supercapacitor displayed a higher areal capacitance of 123.8 mF cm^{-2} (at 5 mV/s) and an energy density of 8.44 μW cm^{-2} with 90% capacitance retention when operated over 10,000 cycles.

OUTLOOK

With a wide variety of compositions of *MXene* materials, they have been identified as the fastest-growing class of 2D materials exhibiting fascinating physical, chemical, and physicochemical properties with promises in many emerging applications. Synthesis fundamentals of *MXene* with an understanding of the structure and chemical compositions of MAX phase and derivation of corresponding *MXene* at the atomic scale have still been dominating the current field of research with the long-term goal of achieving scalable manufacturing with structural stability. However, additive manufacturing to enable *MXene*'s emerging applications has great potential for *MXene*'s future research and development. The beneficial aspects of easy solution-processed *MXene* inks have already highlighted their simplicity and applicability in IJP technology, making an attractive avenue for *MXene*-based printed electronics. The efficient way to implement stable *MXene* colloidal solution into films and/or device architectures using printing technology is still in its infancy. Figure below (Figure 5) shows diverse application domains of *MXene*-based inks. The structure-property-manufacturing applications remain the key aspects of the successful integration of *MXene*-based inks into novel areas of use. All the applications projected in Figure 5 can be adopted via additive manufacturing, such as IJP.

Figure 6 above represents a futuristic roadmap of printed *MXene* research and development. Even though the IJP of *MXene* has been recently demonstrated, each of the projected applications needs different sets of requirements bringing various challenges to understand and address in *MXene* materials.

MXene synthesis

Initially, *MXene* was exfoliated from the parent MAX phase using HF, and since then there have been significant advancements in the synthesis of *MXene*. Different MAX phase materials have been discovered in parallel to create new *MXene* materials. However, due to the complexity of various elemental presence in different MAX phases challenges arise in making a standard synthesis model for *MXene* exfoliation. In addition, countable work has been focused on the properties of exfoliated *MXene* at its atomic and molecular level, however, new understanding in the crystal growth of newer MAX phase materials and exfoliation of corresponding *MXene* will continue to bring new knowledge and open doors for new applications (Figure 5). The physicochemical properties and its device applications of *MXene* in terms of layer structure, functional groups, chemical composition, stacked layer assembly, lateral size, and importantly oxidation stability after device fabrications will remain to be explored

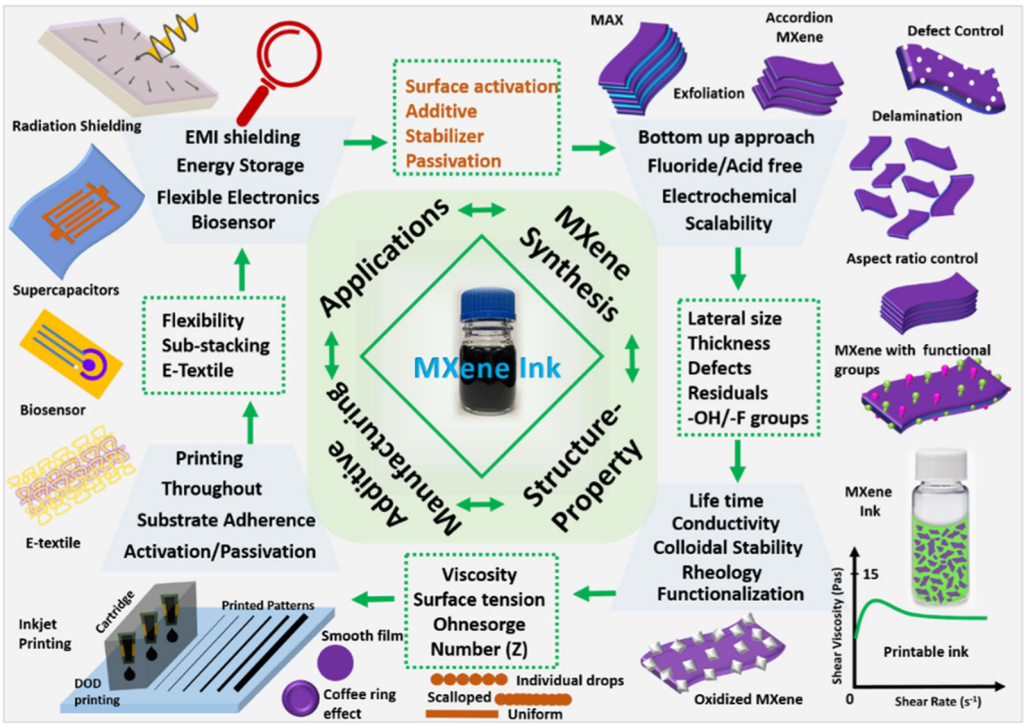

FIGURE 5 Overview of structure-property-manufacturing-application nexus for conductive *MXene* ink synthesis and its IJP leading to various applications.

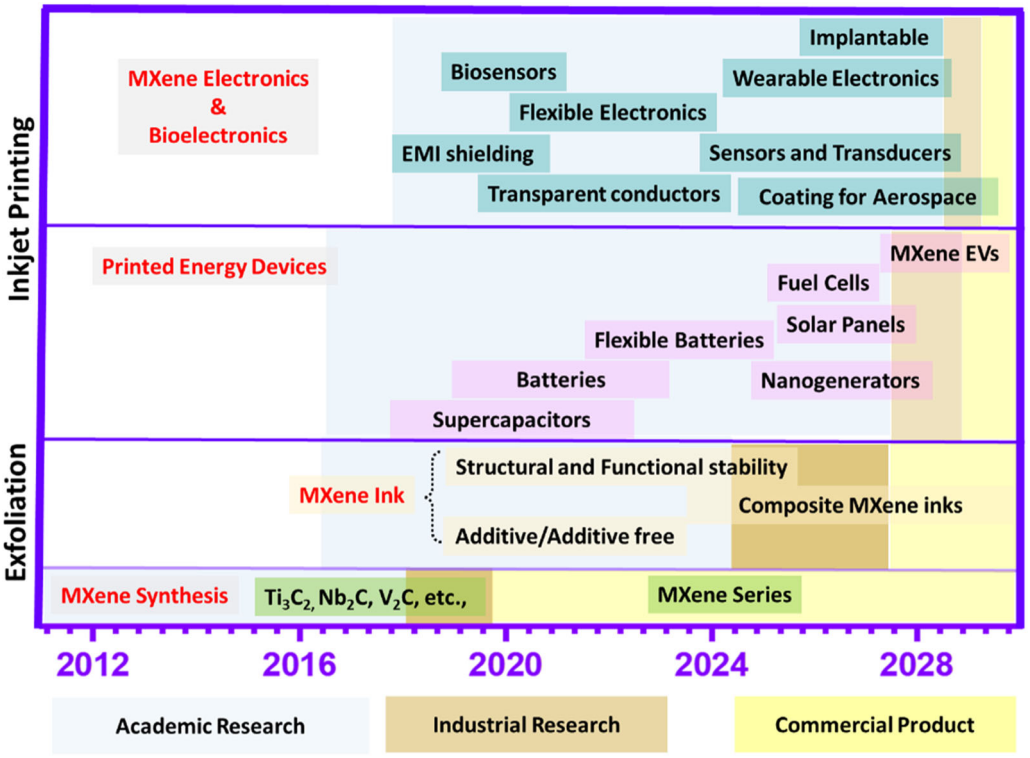

FIGURE 6 Future roadmap of printed *MXene* research and developments leading to emerging applications.

TABLE 2 Comparison of $Ti_3C_2T_x$ *MXene* conductive inks and inks of other popular 2D materials.

2D Material Inks	Solvent	Synthesis route	Additive/Surfactant	Electrical Conductivity/Sheet Resistance	Reference
$Ti_3C_2T_x$	Water	MILD	---^{NA}	1.64 × 10^3 (S/cm)	[100]
$Ti_3C_2T_x$	Water	MILD	Ionic Liquid	0.56 × 10^3 (S/cm)	[100]
$Ti_3C_2T_x$	Water	MILD	Sodium L-ascorbate	5.7 ± 0.5 × 10^2 (S/cm)	[99]
$Ti_3C_2T_x$	Water	MILD	---^{NA}	19,325 (S/cm)	[9]
$Ti_3C_2T_x$	Ethanol	MILD	---^{NA}	2770 (S/cm)	[67]
$Ti_3C_2T_x$	Water	HCl+HF	---^{NA}	4.3 ± 0.1 (Ω/□)	[34]
$Ti_3C_2T_x$	Water	MILD	Graphene	4.28 (S/cm)	[124]
$Ti_3C_2T_x$	Ethanol	MILD	Trifluoroacetic acid	8900 (S/cm)	[130]
Graphene	Cyclohexanone and Terpineol	---ND	---^{NA}	209.1 (Ω/□)	[131]
Graphene	Cyclohexanone and Terpineol	LPE	Ethyl Cellulose	80.72 S/cm	[132]
MoS_2	Water	LPE	sodium cholate	4.02 × 10^{-3} S/cm	[133]
CNT	water	---ND	Carboxymethyl cellulose	1.06 (Ω/□)	[134]

Abbreviations: LPE, Liquid Phase Exfoliation; MILD, Minimal Intensive layer delamination; NA, No additive; ND, No Data.

and addressed. Apart from a recent report by Shuck et al., [64] a scalable synthesis of *MXene* exfoliation for practical application further requires substantial optimization. Extensive work on factors such as layer separation, delamination, functionalization, and increasing the shelf life of *MXene* employing surface passivation are some of the most important activities of *MXene* research that continue to evolve. Finally, although currently the *MXene* synthesis to start with mostly rely on high quality MAX material growth, transformative material growth techniques that are scalable, controllable in quality, and promise fundamentally to eliminate the chemical etching processes of *MXene* will be the ultimate success. Early stage of chemical vapor deposition (CVD) of *MXene* has been reported and its high yield in future will pave the way for the benign formulation of *MXene* inks [128].

MXene ink

While the formulation of stable and reliable *MXene* suspension is important to the successful demonstration of flexible *MXetronics* and other emerging printed electronics applications, the key to their success is the fundamental understanding of *MXene*-solvent interactions and rheological properties of the colloidal suspension such as ink viscosity, surface tension, zeta potential, and their dynamical properties. Solvent types play vital role that could associate multiple factors mentioned above to design stable *MXene* inks. Depending on the solvent molecules they may directly chemically functionalize the *MXene* surface and passivate from external degradation or they may form a high dielectric layer surrounding the *MXene* flake leading to increased stability. Exploitation of surface negative charges with solvents such as water and organic solvents such as dimethyl sulfoxide (DMSO), N,N-dimethylformamide (DMF), N-methyl-2-pyrrolidone (NMP), and propylene carbonate (PC,) for surfactant-free or additive-free *MXene* inks design [10, 129] while unique to *MXene*, it provides opportunity to engineer the surface chemistry of the ink particles. Controlled flake size, thickness, surface engineering, functionalization, and their impact on the rheology of the inks will have fundamental differences in the ink properties (as schematically shown in Figure 5) and its printing behavior. Despite numerous optimization parameters to get the most physically stable *MXene* ink, retaining the electrical conductivity for the conductive *MXene* ink is the most important challenge one must consider. For example, the electrical conductivity of $Ti_3C_2T_x$ MXene reduces to ~333 S/cm from a reported value of ~2500 S/cm when DMF is used as a solvent instead of water [65]. Though the understanding of controlled synthesis, and physical and chemical properties of *MXene* materials remain as active research areas, stable and reliable *MXene* ink synthesis for printing technology with rheological parameters and dimensionless parameters for IJP *MXene* of reported work have been summarized in Table 1. Note that there is a large deviation of values from each other in the reported work and some of them even do not fit within the theoretical limit, requiring more understanding in the *MXene* ink research. Finally, the development of eco-friendly *MXene* inks involving suitable solvents and chemicals and benign synthesis routes (such as harsh acid-free synthesis from MAX phase) that are suitable for IJP will have a long-term impact on the *MXene*'s practical applications. For comparison with other well-studied 2D-materials, a separate table (Table 2) on 2D material inks has also been provided. Table 2 mostly compares the electrical conductivities of the conductive inks.

MXene IJP

MXene is identified as a newly printable 2D material for IJP technology, however, it requires much further investigation on scalable, reliable, and efficient printing and coating due to the above-mentioned issues in *MXene* ink research. Key printing parameters, precision, printed layer stability, and reliability, including DoD multilayer printing with improved surface roughness, are some of the promises that are yet to come in the future. These will transform the future of *MXetronic* devices for a wide variety of applications as mentioned in the roadmap Figure 6. Multi-material and multi-layer *MXene* IJP involving various *MXene* inks and inks with other 2D materials will further diversify the potential of *MXene*'s IJP science and technology. The present proof-of-concept of printed devices and their applications such as LED, EMI shielding, micro-supercapacitors, photonic devices to biosensor of IJP *MXene* are only the beginning of this research and has the potential to lead to numerous unprecedented new applications in the future.

CONCLUSIONS

In conclusion, the present review provides a comprehensive discussion on *MXene* material inks and their inkjet printing properties for flexible electronics applications in a variety of emerging technologies. The synthesis of tailored *MXene* inks using various solvents with tunable structure, surface functional group, rheology for functional applications with a goal to use them in additive manufacturing for high-resolution and highly stable printed *MXetronics* as a transformational *MXene* research direction has been emphasized. Considering above priorities for printable flexible *MXetronics*, the ambient stability and reliability of *MXene* inks and their printed structures are among the most important factors to achieve for future research and development in this growing research field. *MXene* possesses the highest electrical conductivity among any given 2D atomically thin materials, directly demonstrating its potential success for *MXene* conductive inks. However, presently the conductive *MXene* inks are also mostly limited to the very first member of *MXene* family, that is, to $Ti_3C_xT_x$. Therefore, more research on fundamental understanding of other members of *MXene* family and their interactions with diverse range of solvents, including the ones with environmentally benign in nature, remains a widely open avenue for future *MXene* inks. A systematic understanding and success in synthesis of *MXene* inks and their printing fundamentals will directly benefit the future success of printed and flexible *MXetronics*.

ACKNOWLEDGMENTS

S.R.D. acknowledges support from the U.S. National Science Foundation (NSF) Signals in the Soil (SitS), grant no. NSF CBET # 1935676, to conduct this work.

CONFLICT OF INTEREST STATEMENT

The authors declare no conflict of interest.

DATA AVAILABILITY STATEMENT

This is a mini review. Most of the data are collected from other articles. Figures 5 and 6 are made by the authors. Figure 2 (e) and (f) are constructed from available data in the literature.

REFERENCES

[1] Y. Gogotsi, B. Anasori, *ACS Nano* **2019**, *13*(8), 8491.
[2] Y. Gogotsi, Q. Huang, *ACS Nano* **2021**, *15*(4), 5775.
[3] J. Zhu, S. Wei, J. Tang, Y. Hu, X. Dai, Y. Zi, M. Wang, Y. Xiang, W. Huang, *ACS Appl. Nano Mater.* **2023**, *6*(14), 13629.
[4] M. Wang, J. Zhu, Y. Zi, W. Huang, *ACS Appl. Mater. Interfaces* **2021**, *13*(39), 47302.
[5] C. Wang, J. Xu, Y. Wang, Y. Song, J. Guo, W. Huang, Y. Ge, L. Hu, J. Liu, H. Zhang, *Sci. China Mater.* **2021**, *64*(1), 259.
[6] W. Huang, C. Ma, C. Li, Y. Zhang, L. Hu, T. Chen, Y. Tang, J. Ju, H. Zhang, *Nanophotonics* **2020**, *9*(8), 2577.
[7] W. Huang, L. Hu, Y. Tang, Z. Xie, H. Zhang, *Adv. Funct. Mater.* **2020**, *30*(49), 2005223.
[8] T. Wu, P. R. C. Kent, Y. Gogotsi, D. e Jiang, *Chem. Mater.* **2022**, *34*(11), 4975.
[9] T. Guo, D. Zhou, S. Deng, M. Jafarpour, J. Avaro, A. Neels, J. Heier, C. Zhang, *ACS Nano* **2023**, *17*(4), 3737.
[10] S. Abdolhosseinzadeh, X. Jiang, H. Zhang, J. Qiu, C. Zhang, *Mater. Today* **2021**, *48*, 214.
[11] L. Nayak, S. Mohanty, S. K. Nayak, A. Ramadoss, *J. Mater. Chem. C* **2019**, *7*(29), 8771.
[12] Z. Zhan, J. An, Y. Wei, V. T. Tran, H. Du, *Nanoscale* **2017**, *9*(3), 965.
[13] F. Torrisi, T. Hasan, W. Wu, Z. Sun, A. Lombardo, T. S. Kulmala, G.-W. Hsieh, S. Jung, F. Bonaccorso, P. J. Paul, D. Chu, A. C. Ferrari, *ACS Nano* **2012**, *6*(4), 2992.
[14] J. Li, M. M. Naiini, S. Vaziri, M. C. Lemme, M. Östling, *Adv. Funct. Mater.* **2014**, *24*(41), 6524.
[15] G. Hu, J. Kang, L. W. T. Ng, X. Zhu, R. C. T. Howe, C. G. Jones, M. C. Hersam, T. Hasan, *Chem. Soc. Rev.* **2018**, *47*(9), 3265.
[16] F. Bonaccorso, A. Bartolotta, J. N. Coleman, C. Backes, *Adv. Mater.* **2016**, *28*(29), 6136.
[17] A. Sajedi-Moghaddam, E. Rahmanian, N. Naseri, *ACS Appl. Mater. Interfaces* **2020**, *12*(31), 34487.
[18] H. Kim, H. N. Alshareef, *ACS Mater. Lett.* **2019**, *2*(1), 55.
[19] E. Jabari, F. Ahmed, F. Liravi, E. B. Secor, L. Lin, E. Toyserkani, *2D Mater.* **2019**, *6*(4), 042004.
[20] W. Wu, *Nanoscale* **2017**, *9*(22), 7342.
[21] M. Zeng, Y. Zhang, *J. Mater. Chem. A* **2019**, *7*(41), 23301.
[22] J. Liang, C. Jiang, W. Wu, *Appl. Phys. Rev.* **2021**, *8*(2), 021319.
[23] Y. Gao, X. Guo, Z. Qiu, G. Zhang, R. Zhu, Y. Zhang, H. Pang, *Chem. Phys. Mater.* **2021**.
[24] G. Cummins, M. P. Desmulliez, *Circuit World* **2012**, *38*(4), 193.
[25] B. J. de Gans, P. C. Duineveld, U. S. Schubert, *Adv. Mater.* **2004**, *16*(3), 203.
[26] L. Huang, Y. Huang, J. Liang, X. Wan, Y. Chen, *Nano Res.* **2011**, *4*(7), 675.
[27] A. P. S. Gaur, W. Xiang, A. Nepal, J. P. Wright, P. Chen, T. Nagaraja, S. Sigdel, B. LaCroix, C. M. Sorensen, S. R. Das, *ACS Appl. Energy Mater.* **2021**, *4*(8), 7632.
[28] B. Zazoum, A. Bachri, J. Nayfeh, *Materials* **2021**, *14*(21), 6603.
[29] K. Hassan, M. J. Nine, T. T. Tung, N. Stanley, P. L. Yap, H. Rastin, L. Yu, D. Losic, *Nanoscale* **2020**, *12*(37), 19007.
[30] P. Li, C.-A. Tao, B. Wang, J. Huang, T. Li, J. Wang, *J. Nanosci. Nanotechnol.* **2018**, *18*(1), 713.
[31] D. Zhu, Z. Wang, D. Zhu, *J. Electron. Mater.* **2020**, *49*(3), 1765.
[32] G. Hu, T. Albrow-Owen, X. Jin, A. Ali, Y. Hu, R. C. T. Howe, K. Shehzad, Z. Yang, X. Zhu, R. I. Woodward, T. C. Wu, H. Jussila,

J. B. Wu, P. Peng, P. H. Tan, Z. Sun, E. Kelleher, M. Zhang, Y. Xu, T. Hasan, *Nat. Commun.* **2017**, *8*(1), 278.
[33] W. J. Hyun, L. E. Chaney, J. R. Downing, A. C. M. De Moraes, M. C. Hersam, *Faraday Discuss.* **2021**, *227*, 92.
[34] S. Uzun, M. Schelling, K. Hantanasirisakul, T. S. Mathis, R. Askeland, G. Dion, Y. Gogotsi, *Small* **2021**, *17*(1), 2006376.
[35] H. Lee, M. Koo, C. Park, M. Patel, H. Han, T. H. Park, P. Kumar, W.-G. Koh, C. Park, *Nano Res.* **2020**, *13*(10), 2726.
[36] H. Huang, R. Jiang, Y. Feng, H. Ouyang, N. Zhou, X. Zhang, Y. Wei, *Nanoscale* **2020**, *12*(3), 1325.
[37] H. Shalom, S. Kapishnikov, V. Brumfeld, N. Naveh, R. Tenne, N. Lachman, *Sci. Rep.* **2020**, *10*(1), 8892.
[38] Y. Li, M. Sivan, J. X. Niu, H. Veluri, E. Zamburg, J. Leong, U. Chand, S. Samanta, X. Wang, X. Feng, Aerosol jet printed WSe 2 based RRAM on kapton suitable for flexible monolithic memory integration, in 2019 IEEE International Conference on Flexible and Printable Sensors and Systems (FLEPS), (IEEE, City, 2019), 1.
[39] X. Ma, Z. Xie, Z. Yang, G. Zeng, M. Xue, X. Zhang, *Mater. Res. Express* **2018**, *6*(1), 015025.
[40] Q. Jiang, Y. Lei, H. Liang, K. Xi, C. Xia, H. N. Alshareef, *Energy Storage Mater.* **2020**, *27*, 78.
[41] M. Alhabeb, K. Maleski, B. Anasori, P. Lelyukh, L. Clark, S. Sin, Y. Gogotsi, *Chem. Mater.* **2017**, *29*(18), 7633.
[42] H. Zhang, Z. Wang, F. Wang, Y. Zhang, H. Wang, Y. Liu, *Talanta* **2021**, *224*, 121879.
[43] K. Rajavel, T. Ke, K. Yang, D. Lin, *Nanotechnology* **2018**, *29*(9), 095605.
[44] K. Rajavel, X. Yu, P. Zhu, Y. Hu, R. Sun, C. Wong, *ACS Appl. Mater. Interfaces* **2020**, *12*(44), 49737.
[45] T. Yun, H. Kim, A. Iqbal, Y. S. Cho, G. S. Lee, M.-K. Kim, S. J. Kim, D. Kim, Y. Gogotsi, S. O. Kim, C. M. Koo, *Adv. Mater.* **2020**, *32*(9), 1906769.
[46] K. Rajavel, S. Shen, T. Ke, D. Lin, *2D Mater.* **2019**, *6*(3), 035040.
[47] A. Thakur, N. Chandran BS, K. Davidson, A. Bedford, H. Fang, Y. Im, V. Kanduri, B. C. Wyatt, S. K. Nemani, V. Poliukhova, R. Kumar, Z. Fakhraai, B. Anasori, *Small Methods* **2023**, *7*, 2300030.
[48] C. Zhang, B. Anasori, A. Seral-Ascaso, S. H. Park, N. McEvoy, A. Shmeliov, G. S. Duesberg, J. N. Coleman, Y. Gogotsi, V. Nicolosi, *Adv. Mater.* **2017**, *29*(36), 1702678.
[49] M. Pandey, K. S. Thygesen, *J. Phys. Chem. C* **2017**, *121*(25), 13593.
[50] A. Lipatov, H. Lu, M. Alhabeb, B. Anasori, A. Gruverman, Y. Gogotsi, A. Sinitskii, *Sci. Adv.* **2018**, *4*(6), eaat0491.
[51] V. N. Borysiuk, V. N. Mochalin, Y. Gogotsi, *Nanotechnology* **2015**, *26*(26), 265705.
[52] Y. Dong, S. Chertopalov, K. Maleski, B. Anasori, L. Hu, S. Bhattacharya, A. M. Rao, Y. Gogotsi, V. N. Mochalin, R. Podila, *Adv. Mater.* **2018**, *30*(10), 1705714.
[53] X.-H. Zha, Q. Huang, J. He, H. He, J. Zhai, J. S. Francisco, S. Du, *Sci. Rep.* **2016**, *6*(1), 27971.
[54] M. K. Aslam, M. Xu, *Nanoscale* **2020**, *12*(30), 15993.
[55] M. Hu, H. Zhang, T. Hu, B. Fan, X. Wang, Z. Li, *Chem. Soc. Rev.* **2020**, *49*(18), 6666.
[56] F. Shahzad, M. Alhabeb, C. B. Hatter, B. Anasori, S. Man Hong, C. M. Koo, Y. Gogotsi, *Science* **2016**, *353*(6304), 1137.
[57] T. Zhao, C. Liu, C. Zhao, W. Xu, Y. Liu, I. Z. Mitrovic, E. G. Lim, L. Yang, C. Z. Zhao, *J. Mater. Chem. A* **2021**, *9*(32), 17390.
[58] Z. Liu, H. N. Alshareef, *Adv. Electron. Mater.* **2021**, *7*(9), 2100295.
[59] H. Xu, A. Ren, J. Wu, Z. Wang, *Adv. Funct. Mater.* **2020**, *30*(24), 2000907.
[60] S. Mehdi Aghaei, A. Aasi, B. Panchapakesan, *ACS Omega* **2021**, *6*(4), 2450.
[61] Q. A. Zahra, S. Ullah, F. Shahzad, B. Qiu, X. Fang, A. Ammar, Z. Luo, S. Abbas Zaidi, *Prog. Mater. Sci.* **2022**, *129*, 100967.
[62] S. Iravani, R. S. Varma, *ACS Biomater. Sci. Eng.* **2021**, *7*(6), 1900.
[63] Y. Z. Zhang, Y. Wang, Q. Jiang, J. K. El-Demellawi, H. Kim, H. N. Alshareef, *Adv. Mater.* **2020**, *32*(21), 1908486.
[64] C. E. Shuck, A. Sarycheva, M. Anayee, A. Levitt, Y. Zhu, S. Uzun, V. Balitskiy, V. Zahorodna, O. Gogotsi, Y. Gogotsi, *Adv. Eng. Mater.* **2020**, *22*(3), 1901241.
[65] Q. Zhang, H. Lai, R. Fan, P. Ji, X. Fu, H. Li, *ACS Nano* **2021**, *15*(3), 5249.
[66] K. Maleski, V. N. Mochalin, Y. Gogotsi, *Chem. Mater.* **2017**, *29*(4), 1632.
[67] C. Zhang, L. McKeon, M. P. Kremer, S.-H. Park, O. Ronan, A. Seral-Ascaso, S. Barwich, C. Ó. Coileáin, N. McEvoy, H. C. Nerl, B. Anasori, J. N. Coleman, Y. Gogotsi, V. Nicolosi, *Nat. Commun.* **2019**, *10*(1), 1795.
[68] B. Akuzum, K. Maleski, B. Anasori, P. Lelyukh, N. J. Alvarez, E. C. Kumbur, Y. Gogotsi, *ACS Nano* **2018**, *12*(3), 2685.
[69] S. P. Sreenilayam, I. Ul Ahad, V. Nicolosi, D. Brabazon, *Mater. Today* **2021**, *43*, 99.
[70] M. Greaves, M. Mende, J. Wang, W. Yang, S. Barg, *J. Mater. Res.* **2021**, *36*(22), 4578.
[71] P. Urbankowski, B. Anasori, T. Makaryan, D. Er, S. Kota, P. L. Walsh, M. Zhao, V. B. Shenoy, M. W. Barsoum, Y. Gogotsi, *Nanoscale* **2016**, *8*(22), 11385.
[72] T. S. Mathis, K. Maleski, A. Goad, A. Sarycheva, M. Anayee, A. C. Foucher, K. Hantanasirisakul, C. E. Shuck, E. A. Stach, Y. Gogotsi, *ACS Nano* **2021**, *15*(4), 6420.
[73] M. Naguib, O. Mashtalir, J. Carle, V. Presser, J. Lu, L. Hultman, Y. Gogotsi, M. W. Barsoum, *ACS Nano* **2012**, *6*(2), 1322.
[74] W. Hong, B. C. Wyatt, S. K. Nemani, B. Anasori, *MRS Bull.* **2020**, *45*(10), 850.
[75] J. Jiang, S. Bai, J. Zou, S. Liu, J.-P. Hsu, N. Li, G. Zhu, Z. Zhuang, Q. Kang, Y. Zhang, *Nano Res.* **2022**, *15*, 6551.
[76] C. E. Shuck, K. Ventura-Martinez, A. Goad, S. Uzun, M. Shekhirev, Y. Gogotsi, *ACS Chem. Health Safety* **2021**, *28*(5), 326.
[77] K. Matthews, T. Zhang, C. E. Shuck, A. VahidMohammadi, Y. Gogotsi: Guidelines for Synthesis and Processing of Chemically Stable Two-Dimensional V2CT x MXene *Chem. Mater.* **2021**.
[78] A. Lipatov, M. Alhabeb, M. R. Lukatskaya, A. Boson, Y. Gogotsi, A. Sinitskii, *Adv. Electron. Mater.* **2016**, *2*(12), 1600255.
[79] O. Mashtalir, M. Naguib, V. N. Mochalin, Y. Dall'Agnese, M. Heon, M. W. Barsoum, Y. Gogotsi, *Nat. Commun.* **2013**, *4*(1), 1716.
[80] S. Shen, T. Ke, K. Rajavel, K. Yang, D. Lin, *Small* **2020**, *16*(36), 2002433.
[81] A. Feng, Y. Yu, F. Jiang, Y. Wang, L. Mi, Y. Yu, L. Song, *Ceramics Int.* **2017**, *43*(8), 6322.
[82] A. Shayesteh Zeraati, S. A. Mirkhani, P. Sun, M. Naguib, P. V. Braun, U. Sundararaj, *Nanoscale* **2021**, *13*(6), 3572.
[83] H. Aghamohammadi, A. Heidarpour, R. Jamshidi, S. Ghasemi, *Adv. Powder Technol.* **2019**, *30*(2), 393.
[84] S. Yang, P. Zhang, F. Wang, A. G. Ricciardulli, M. R. Lohe, P. W. M. Blom, X. Feng, *Angew. Chem.* **2018**, *130*(47), 15717.
[85] H. L. Chia, C. C. Mayorga-Martinez, N. Antonatos, Z. Sofer, J. J. Gonzalez-Julian, R. D. Webster, M. Pumera, *Anal. Chem.* **2020**, *92*(3), 2452.
[86] J. Wang, S. Liu, Y. Wang, T. Wang, S. Shang, W. Ren, *J. Mater. Chem. C* **2020**, *8*(5), 1608.
[87] C. E. Shuck, M. Han, K. Maleski, K. Hantanasirisakul, S. J. Kim, J. Choi, W. E. B. Reil, Y. Gogotsi, *ACS Appl. Nano Mater.* **2019**, *2*(6), 3368.
[88] K. Rajavel, X. Yu, P. Zhu, Y. Hu, R. Sun, C. Wong, *J. Alloys Compd.* **2021**, *877*, 160235.
[89] O. Mashtalir, M. R. Lukatskaya, M. Q. Zhao, M. W. Barsoum, Y. Gogotsi, *Adv. Mater.* **2015**, *27*(23), 3501.
[90] X. Sang, Y. Xie, M.-W. Lin, M. Alhabeb, K. L. Van Aken, Y. Gogotsi, P. R. C. Kent, K. Xiao, R. R. Unocic, *ACS Nano* **2016**, *10*(10), 9193.
[91] F. Xia, J. Lao, R. Yu, X. Sang, J. Luo, Y. Li, J. Wu, *Nanoscale* **2019**, *11*(48), 23330.

[92] R. Khaledialidusti, A. K. Mishra, A. Barnoush, *J. Mater. Chem. C* **2020**, *8*(14), 4771.
[93] V. Parey, B. M. Abraham, S. H. Mir, J. K. Singh, *ACS Appl. Mater. Interfaces* **2021**, *13*(30), 35585.
[94] A. Iqbal, J. Hong, T. Y. Ko, C. M. Koo, *Nano Convergence* **2021**, *8*(1), 9.
[95] C. J. Zhang, S. Pinilla, N. McEvoy, C. P. Cullen, B. Anasori, E. Long, S.-H. Park, A. Seral-Ascaso, A. Shmeliov, D. Krishnan, C. Morant, X. Liu, G. S. Duesberg, Y. Gogotsi, V. Nicolosi, *Chem. Mater.* **2017**, *29*(11), 4848.
[96] M. Malaki, A. Maleki, R. S. Varma, *J. Mater. Chem. A* **2019**, *7*(18), 10843.
[97] X. Zhao, A. Vashisth, J. W. Blivin, Z. Tan, D. E. Holta, V. Kotasthane, S. A. Shah, T. Habib, S. Liu, J. L. Lutkenhaus, M. Radovic, M. J. Green, *Adv. Mater. Interfaces* **2020**, *7*(20), 2000845.
[98] M. Carey, Z. Hinton, V. Natu, R. Pai, M. Sokol, N. J. Alvarez, V. Kalra, M. W. Barsoum, *Cell Reports Phys. Sci.* **2020**, *1*(4), 100042.
[99] X. Zhao, A. Vashisth, E. Prehn, W. Sun, S. A. Shah, T. Habib, Y. Chen, Z. Tan, J. L. Lutkenhaus, M. Radovic, M. J. Green, *Matter* **2019**, *1*(2), 513.
[100] Y.-J. Wan, K. Rajavel, X.-M. Li, X.-Y. Wang, S.-Y. Liao, Z.-Q. Lin, P.-L. Zhu, R. Sun, C.-P. Wong, *Chem. Eng. J.* **2021**, *408*, 127303.
[101] V. Natu, J. L. Hart, M. Sokol, H. Chiang, M. L. Taheri, M. W. Barsoum, *Angew. Chem.* **2019**, *131*(36), 12785.
[102] G. S. Lee, T. Yun, H. Kim, I. H. Kim, J. Choi, S. H. Lee, H. J. Lee, H. S. Hwang, J. G. Kim, D. Kim, H. M. Lee, C. M. Koo, S. O. Kim, *ACS Nano* **2020**, *14*(9), 11722.
[103] B. Bakthavatchalam, K. Habib, R. Saidur, N. Aslfattahi, A. Rashedi, *Appl. Sci.* **2020**, *10*(24), 8943.
[104] F. Cao, Y. Zhang, H. Wang, K. Khan, A. K. Tareen, W. Qian, H. Zhang, H. Ågren, *Adv. Mater.* **2022**, *34*(13), 2107554.
[105] Y. Huang, H. Wu, L. Xiao, Y. Duan, H. Zhu, J. Bian, D. Ye, Z. Yin, *Mater. Horizons* **2019**, *6*(4), 642.
[106] T. Boland, T. Xu, B. Damon, X. Cui, *Biotechnol. J.* **2006**, *1*(9), 910.
[107] M. Singh, H. M. Haverinen, P. Dhagat, G. E. Jabbour, *Adv. Mater.* **2010**, *22*(6), 673.
[108] P. Calvert, *Chem. Mater.* **2001**, *13*(10), 3299.
[109] J. Li, F. Ye, S. Vaziri, M. Muhammed, M. C. Lemme, M. Östling, *Adv. Mater.* **2013**, *25*(29), 3985.
[110] E. B. Secor, P. L. Prabhumirashi, K. Puntambekar, M. L. Geier, M. C. Hersam, *J. Phys. Chem. Lett.* **2013**, *4*(8), 1347.
[111] J. R. Castrejón-Pita, G. D. Martin, S. D. Hoath, I. M. Hutchings, *Rev. Sci. Instrum.* **2008**, *79*(7), 075108.
[112] D. Jang, D. Kim, J. Moon, *Langmuir* **2009**, *25*(5), 2629.
[113] B. Derby, *Annu. Rev. Mater. Res.* **2010**, *40*, 395.
[114] H. Hu, R. G. Larson, *J. Phys. Chem. B* **2006**, *110*(14), 7090.
[115] S. I. Karakashev, R. Tsekov, *Langmuir* **2011**, *27*(6), 2265.
[116] Y. Pang, Y. Cao, Y. Chu, M. Liu, K. Snyder, D. MacKenzie, C. Cao, *Adv. Funct. Mater.* **2020**, *30*(1), 1906244.
[117] M. Vural, A. Pena-Francesch, J. Bars-Pomes, H. Jung, H. Gudapati, C. B. Hatter, B. D. Allen, B. Anasori, I. T. Ozbolat, Y. Gogotsi, M. C. Demirel, *Adv. Funct. Mater.* **2018**, *28*(32), 1801972.
[118] J. Zheng, J. Diao, Y. Jin, A. Ding, B. Wang, L. Wu, B. Weng, J. Chen, *J. Electrochem. Soc.* **2018**, *165*(5), B227.
[119] X. Jiang, W. Li, T. Hai, R. Yue, Z. Chen, C. Lao, Y. Ge, G. Xie, Q. Wen, H. Zhang, *NPJ 2D Mater. Appl.* **2019**, *3*(1), 1.
[120] C.-W. Wu, B. Unnikrishnan, I.-W. P. Chen, S. G. Harroun, H.-T. Chang, C.-C. Huang, *Energy Storage Mater.* **2020**, *25*, 563.
[121] A. Saleh, S. Wustoni, E. Bihar, J. K. El-Demellawi, Y. Zhang, A. Hama, V. Druet, A. Yudhanto, G. Lubineau, H. N. Alshareef, S. Inal, *J. Phys. Mater.* **2020**, *3*(4), 044004.
[122] Y. Wang, M. Mehrali, Y.-Z. Zhang, M. A. Timmerman, B. A. Boukamp, P.-Y. Xu, J. E. ten Elshof, *Energy Storage Mater.* **2021**, *36*, 318.
[123] D. Wen, X. Wang, L. Liu, C. Hu, C. Sun, Y. Wu, Y. Zhao, J. Zhang, X. Liu, G. Ying, *ACS Appl. Mater. Interfaces* **2021**, *13*(15), 17766.
[124] D. Wen, G. Ying, L. Liu, Y. Li, C. Sun, C. Hu, Y. Zhao, Z. Ji, J. Zhang, X. Wang, *J. Alloys Compd.* **2022**, *900*, 163436.
[125] J. Ma, S. Zheng, Y. Cao, Y. Zhu, P. Das, H. Wang, Y. Liu, J. Wang, L. Chi, S. Liu, Z. Wu, *Adv. Energy Mater.* **2021**, *11*(23), 2100746.
[126] E. Gibertini, F. Lissandrello, L. Bertoli, P. Viviani, L. Magagnin, *Coatings* **2023**, *13*(2), 230.
[127] G. Wang, R. Zhang, H. Zhang, K. Cheng, *J. Colloid Interface Sci.* **2023**, *645*, 359.
[128] D. Wang, C. Zhou, A. S. Filatov, W. Cho, F. Lagunas, M. Wang, S. Vaikuntanathan, C. Liu, R. F. Klie, D. V. Talapin, *Science* **2023**, *379*(6638), 1242.
[129] V. Kamysbayev, A. S. Filatov, H. Hu, X. Rui, F. Lagunas, D. Wang, R. F. Klie, D. V. Talapin, *Science* **2020**, *369*(6506), 979.
[130] X. Tang, G. Murali, H. Lee, S. Park, S. Lee, S. M. Oh, J. Lee, T. Y. Ko, C. M. Koo, Y. J. Jeong, T. K. An, I. In, S. H. Kim, *Adv. Funct. Mater.* **2021**, *31*(29), 2010897.
[131] M. R. Ahmed, W. Mirihanage, P. Potluri, A. Fernando, *Part. Part. Syst. Charact.* **2023**, *40*(2), 2200153.
[132] T. Nagaraja, R. Krishnamoorthy, K. M. Asif Raihan, B. Lacroix, S. R. Das, *ACS Appl. Nano Mater.* **2023**, *6*(21), 20288.
[133] P. Ni, M. Dieng, J.-C. Vanel, I. Florea, F. Z. Bouanis, A. Yassar, *Nanomaterials* **2023**, *13*(18), 2502.
[134] N. Gupta, D. Kumar, A. Das, S. Sood, B. D. Malhotra, *New J. Chem.* **2023**, *47*(23), 10930.

How to cite this article: R. Krishnamoorthy, S. R. Das, *Appl. Res.* **2024**;*3*:e202300085.
https://doi.org/10.1002/appl.202300085